Experimentation, Characterization and Enhancement of an Automated Fiber Optic Gyroscope Coil Winding Machine

By

Min-Hong Tsai

B.S., Mechanical Engineering 1996
University of Illinois, Champaign-Urbana

Submitted to the Department of Mechanical Engineering
in Partial Fulfillment of the Requirements for the Degree of

Master of Science in Mechanical Engineering
At the
Massachusetts Institute of Technology

June 1998

Signature of Author.....
Department of Mechanical Engineering
May 7, 1998

Certified by.....
Dr. Andre Sharon
Executive Officer of the Manufacturing Institute
Thesis Supervisor

Accepted By.....
Ain A. Sonin
Chairman, Department Committee on Graduate Studies

Experimentation, Characterization and Enhancement of an Automated Fiber Optic Gyroscope Coil Winding Machine

by

Min-Hong Tsai

Submitted to the Department of Mechanical Engineering
on May 7, 1998 in Partial Fulfillment of the
Requirements for the Degree of Master of Science in
Mechanical Engineering

ABSTRACT

Since the first proposed use of the fiber optic gyroscope FOG, in the mid 1970's, issues surrounding noise and error have been resolved or reduced. These improvements have made the FOG more accurate and reliable. Its solid state configuration provides distinct advantages over traditional mechanical gyroscopes. However, manufacturing cost remains particularly high. The MIT Manufacturing Institute has recently, developed an automated machine to manufacture optical coils of FOGs. Winding tension is an important area that needed further characterization.

A second machine was developed, with enhanced tension control capability, for winding strategic-grade coils. This thesis describes the development of this machine with an emphasis placed on tension control. The importance of tension control has led to the development of a model to characterize the tension control system. Simulations were conducted in order to gain a better understanding of the dynamics of the system. Finally, experiments on the completed machine were carried out to investigate tension control alternatives and to document the performance of the machine.

Thesis Supervisor: Dr. Andre Sharon
Title: Executive Office of the Manufacturing Institute Laboratory

Acknowledgements

Dr. Andre Sharon, thank you for giving me an opportunity to work on this project. I appreciate the freedom and guidance you have given to me.

Jesse, what can I say? I could never wish for a more enjoyable and creative partner to work with. I'm going to buy a Ben Lee album after I leave here.

Sieu, thanks for keeping the lab lively and keeping us on our toes. Thanks for the generosity you've shown through your cookies and precious time. Guys, remember the good old days when Sieu was working on the vision system? Show me the money!

Pankaj and Tang, I'm glad you guys came on board this year. Thanks for being such great friends. I really enjoyed working, eating and snowboarding with you guys.

Dave and Wayne, thanks for not dropping any weights on me. Seriously though, thanks for all the good times.

Steve and Brian, thank you for having enough patience to answer the hundreds of question that I had when I first arrived. I owe much of what I've learned here from you two.

Jason, thanks for being supportive when I made some dumb mistakes. Good luck with your next machine.

To all of the above, thanks for being like a family away from home.

My family, thanks for your support, encouragement and love.

Table of Contents

1 Introduction 5
1.1 Gyroscopes 5
1.2 Theory of Operation 7
1.3 IFOG Configuration 10
1.4 Coil Winding Issues 11
1.4.1 Mechanically Induced errors 11
1.4.2 Thermally Induced Errors 15
2 Proposed Coil Winder 20
2.1 Current Coil Winding Methods 20
2.2 Proposed Winder 20
2.2.1 Flexibility in Design 21
2.2.2 Supply Unit and Tension Control 23
2.2.3 User Interface 25
3 New Machine 27
3.1 Supply Unit Redesign 28
3.2 Active Ride System 30
3.3 Electrical and Software enhancements 30
3.4 Tension Control States 35
3.5 Ride Tension Control 36
4 Active Tension Control 43
4.1 Simulation 44
4.1.1 Bond Graph 46
4.1.2 Simulink Model 49
4.1.3 Simulation results 50
4.2 Feedforward Control alternative 59
4.2.1 Theory 59
4.2.2 Feed forward Simulink Model 61
4.2.3 Simulink results 61
4.3 Experimental Results 64
4.3.1 Sensor Noise 65
4.3.2 PID Results 68
4.3.3 Feedforward results 70
5 Conclusion 76
6 References 78

1 Introduction

1.1 Gyroscopes

Gyroscopes can be found in almost all modern airplanes, ships and missiles. These sensors provide information on position, attitude and absolute position by providing a directional reference. Without gyroscopes, simple tasks such as aircraft attitude indication to sophisticated applications such as satellite inertial navigation could not be realized.

Traditionally, gyroscopes have been mechanical devices that measure the rate of rotation in inertial space. The operation of mechanical gyros is based on the conservation of momentum of a spinning mass. Applying a calibrated torque to the spinning mass results in a known rate of precession. Precession is the rotation of the angular momentum vector with respect to inertial space. A velocity sensor within the gyroscope measures the rate of rotation of the spinning mass with respect to the vehicle. The difference between the measured mass's rate of rotation with respect to the vehicle and the calculated rate of rotation with respect to inertial space gives the rate of rotation of the vehicle. So by measuring the rotation of the spinning mass with respect to the gyroscope's housing, the rate of rotation of the vehicle can be determined [Wrigley, et al].

Although mechanical gyros have become more accurate and precise devices, they still have major disadvantages inherent in their design. A major source of limitation is the moving parts used in construction of the gimbals and rotor that make up mechanical gyros. Moving parts make these gyros prone to mechanical failure. Regular maintenance

is required to keep the gyro in proper working condition. As with most mechanical devices with moving parts, a warm-up time is also necessary to insure a more accurate and consistent reading.

In search of a more robust design, optic-based gyroscopes have been developed. These solid state devices offer significant improvements in reliability, size, weight, and accuracy. Optic gyroscopes all have a closed loop in which light can travel. Two primary types of optic gyroscopes are Ring Laser Gyroscopes (RLG), which forms a closed loop of light with mirrors and Fiber Optic Gyroscopes (FOG), which utilize optical fiber in order to guide the light. Ring Laser Gyroscopes, the more mature of the two gyroscopes, have been able to achieve high enough precision for inertial navigation. A drawback of the RLG is the production of the lock-in phenomena, which requires dithering to remain sensitive at small rotation rates [Dakin, Culshaw].

FOGs, on the other hand, do not exhibit lock-in phenomena and possess a true solid state configuration. First proposed in the mid 1970's, the FOG was introduced as a promising technology that would improve the sensitivity, weight, and ruggedness of optical gyroscopes by using a multi-turn configuration. As the noise and accuracy of the FOG improved with the development of high quality, low loss fiber, the FOG has become as competitive as other gyroscope technologies. After 20 years of research and development, almost all noise and error obstacles have been cleared, giving the FOG the ability to serve in traditional applications onboard airborne and maritime vehicles. One recent application of FOG is its service in modern aircraft such as the Boeing 777. Because of cost and size advantages, FOGs are now making a head way into new fields

of application, including automobile navigation, robotic control, autonomous vehicle control and oil drilling.

Cost limits the FOG from entering even more commercial and industrial applications. By developing new manufacturing processes, the cost of components and that of the FOG, can be reduced. These efforts can make the use of FOGs more prevalent and economical.

1.2 Theory of Operation

All optical gyroscopes are based on the Sagnac effect. Two counter-propagating light beams travelling via a closed loop will experience a difference in path length in a rotating frame [Krohn]. In Figure 1.1, particles travelling along the perimeter of a disk are used to describe the phenomena. An example of the Sagnac phenomena is shown in the figure below.

(a)

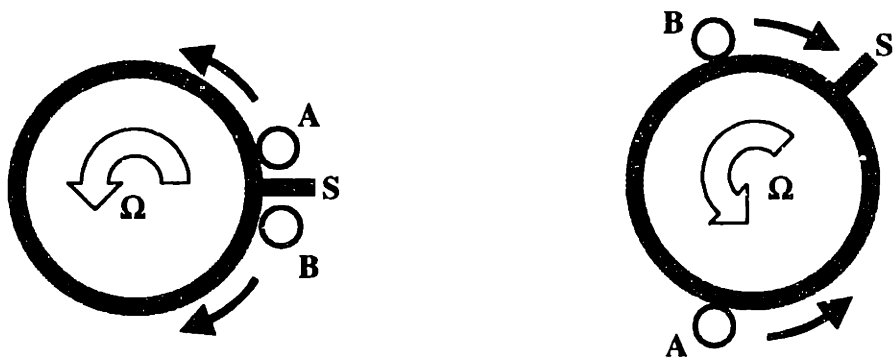

(b)

Figure 1.1 Counter Propagating Light Beams on the perimeter of a (a) stationary and (b) rotary disk.

Assume that particles A and B travel at some velocity along the perimeter of the disk. In the first case where the disk is stationary, both particles will reach the starting point at the same time and experience no difference in path length. In the second case, the disk will rotate at an angular velocity of Ω in a counterclockwise direction. Since the starting point, S, is now moving away from its initial position, particle B will reach point S before particle A. To reach the end point, particle A must travel further than B, thus particles A and B experience a path length difference. This is because the relative velocity between the disk and particle B is faster than that of particle A. The relationship

between the path length difference [ΔL] of the two light beams and the rate of rotation [Ω] is given by

$$\Delta L = \frac{4A}{C_0}\Omega \tag{1}$$

Where A is the area within the fiber-optic loop in the FOG and C_0 is the velocity of light in a vacuum [Burns].

For optical setups, the path length difference will result in a phase shift. In FOGs, a light beam of a known frequency is split and enters the fiber optic loop. If the loop is rotating, the light waves will exit the loop with a path length difference and thus be out of phase. This phase difference [Δϕ] can then be measured to obtain the rate of rotation with the following relationship,

$$\Delta\phi = \frac{2\pi}{\lambda_0}\Delta L = \frac{8\pi A}{\lambda_0 C_0}\Omega \tag{2}$$

Where λ_0 is the wavelength of the light in a vacuum [Burns]. A single optical loop of a FOG gives a phase shift of $3\text{x}10^{-13}$ radians when rotating at 0.01 degree/hr. To improve the sensitivity, multiple loops can be added to magnify the Sagnac effect. For a multi-loop configuration, the new effective area is equal to $A_E = N \cdot A$ where N is the number of loops of a FOG. Therefore, from equations (1) and (2), a coil with N loops will have a

path length difference and phase shift which are both increased by a factor of N. This results in a more sensitive device.

1.3 IFOG Configuration

The configuration of a typical high grade Interferometer gyroscope (IFOG) is shown in the Figure 1.2 below. The components that make up the IFOG include the light source, source splitter, photo detector, integrated optical chip and fiber coil. The light source is typically a laser diode that emits a constant coherent light beam. The light is then routed to the integrated optical chip (IOC) by the source splitter. Within the IOC, the light travels through a polarizer and phase modulators which help reduce noise and increase the sensitivity of the IFOG. After passing though the fiber optic coil, the light recombines and is routed to the photo detector. A shift in phase causes a change in light intensity that is read by the photo detector.

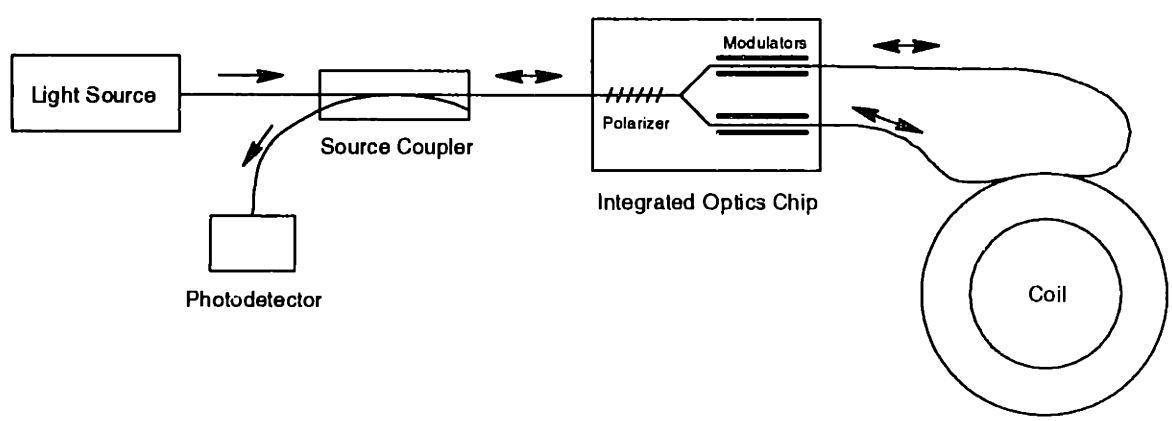

Figure 1.2 IFOG Configuration, used with permission of author [Lin].

1.4 Coil Winding Issues

At the heart of all FOGs is the fiber optic coil that serves to create and magnify the Sagnac Effect. A significant increase in performance can be derived by improving the quality of the FOG coil. Coils are generally categorized into three performance grades in terms of drift. Drift is the rotational error measured in degrees per hour. The lowest grade coils are tactical grade with at least 1°/hr of drift. Navigational grade requires less than 0.1°/hr. In the most demanding applications, such as spacecraft and satellites, strategic grade coils having less than 0.01°/hr of drift are used.

Unlike other phase-modulated sensors, a reference fiber is not required. In a FOG, the two signals being compared will travel along the same fiber. For this configuration, the concept of reciprocity is critical. Reciprocity states that light originating from a single source should exit both ends of the coil with exactly the same phase. For example, if one section of the coil experiences a time independent expansion, the counter-propagating light beams will still experience the same travel distance. Therefore, no phase shift will result. The reciprocity of the coil suggests stronger resistance to environmental disturbances. However, in the presence of non-reciprocal effects a phase shift is detected, resulting in erroneous data. The two most common sources of non-reciprocity are mechanical and temperature related effects.

1.4.1 Mechanically Induced errors

High stress and tension levels in optical fibers results in attenuation and polarization effects. Attenuation is defined by the following relationship,

$$A = -10 \log \frac{P_i}{P_o} \tag{3}$$

Where A is the Attenuation, P_i is the input power and P_o is the output power. Mechanisms of attenuation include absorption, scattering, microgending, and end loss due to reflection. These factors depend heavily of fiber quality and manufacting. However, attenuation can also be a result of excessive bending of fiber [Krohn]. From Snell's law, total internal reflection occurs when the angle of incidence of the light beam is greater than that of the critical angle. In Figure 1.3 the critical angle is reduced by delta at the point in which the fiber begins to bend.

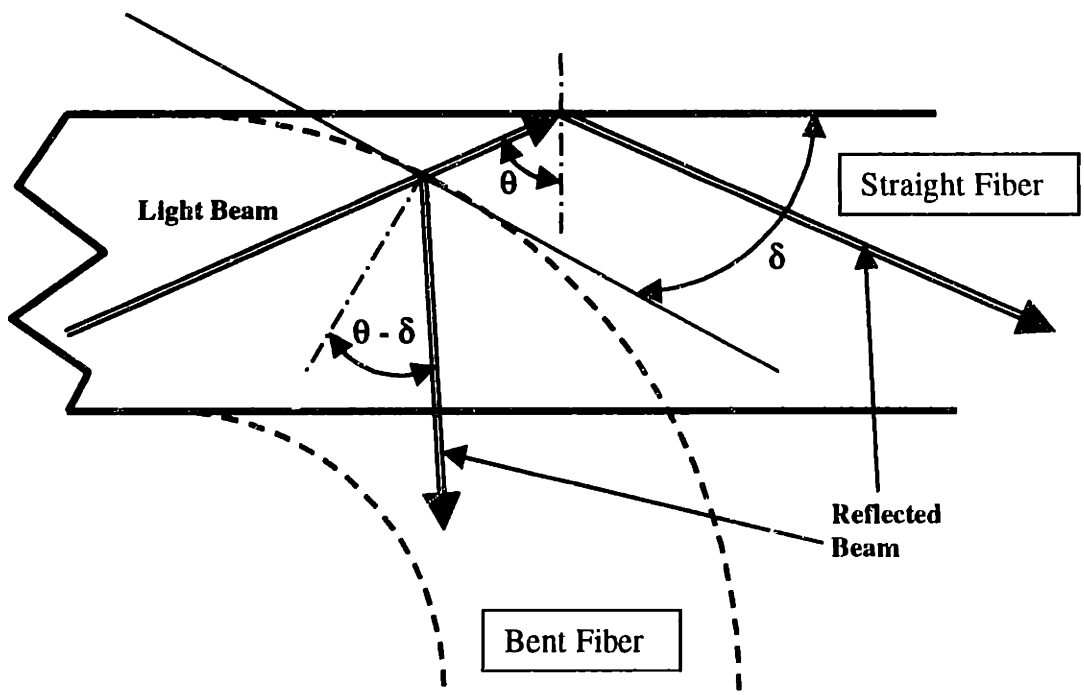

Figure 1.3 Attenuation from Bending of Fiber.

Small amounts of light escape due to the increased likelihood of light transmission versus light reflection.

Another source of error caused by physical deformation and stress is polarization effects. Applying stress on an optical fiber changes the index of refraction of the fiber in the direction of the applied stress. If stress is not applied uniformly around the circumference of the fiber, light traveling along the polarized axis travels at a slower velocity than the other light. This difference in the index of refraction is called bifringence. Bifringence results from high tension levels and localized stresses. Thus, care must be taken to maintain low tension levels and to minimize fiber deformation and coil structure irregularities.

In order to reduce the number of irregularities that introduce stress and bending to the fiber, an orderly and compact winding plan is needed. A popular winding scheme is a helical wind shown in Figure 1.4. In this pattern the fiber is allowed to cross over the underlying fiber at random locations around the turn. When a crossover or jog occurs, the fiber is raised from a valley created by the fiber pack below. The small bumps formed will become increasingly pronounced as the number of layers increase, causing gaps or bumps to form. In the presence of these gaps and bumps, the fiber becomes subject to small radius bends and applied stresses.

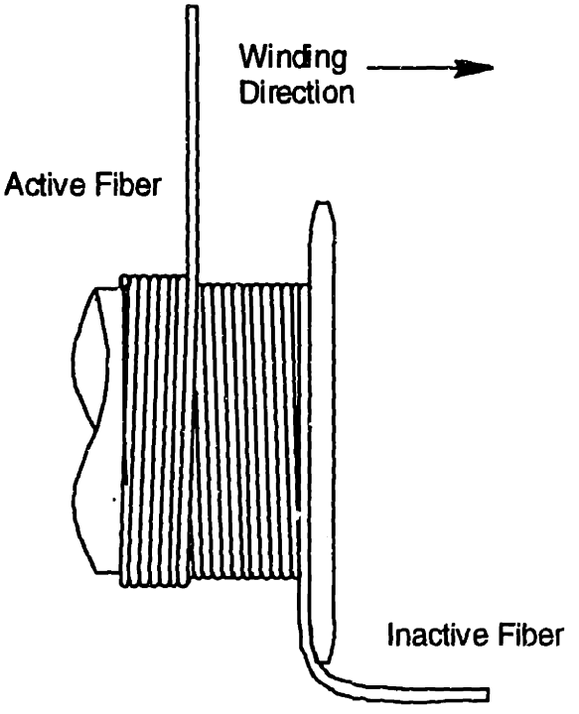

Figure 1.4 Helical Wind [Lin].

A more consistent and organized pattern is the orthocyclic wind shown in Figure 1.5. For this pattern, fiber is wound perpendicular to the axis of the coil and is only allowed to deviate and cross over in a 15-40 degree area called the "jog zone". By restricting the jog zone to a small portion of the coil, the majority of the coil will rest in a lattice-like structure. Overall, the coil will have a more compact configuration with fewer gaps and bumps and with less stress applied onto the fiber. The close pack of the orthocyclic wind also decreases the coil's sensitivity towards thermal variations and mechanical vibrations.

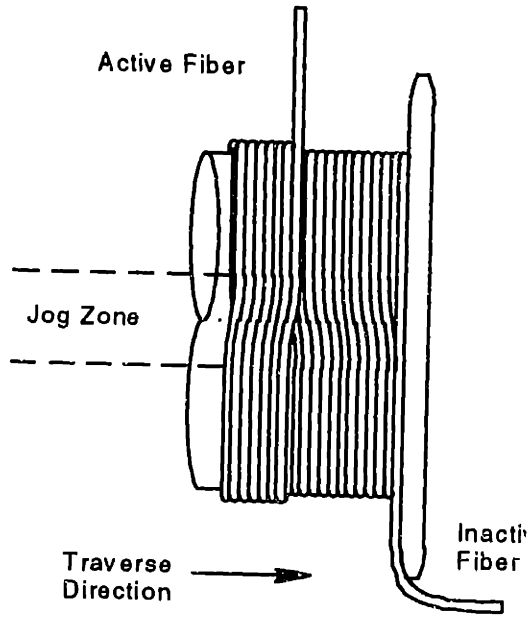

Figure 1.5 Orthocyclic Wind [Lin].

1.4.2 Thermally Induced Errors

Time-dependant thermal effects introduce non-reciprocity in the coil by changing the length of the optical path. A path length difference exists between two signals if a section of the coil expands when light travels through it in one direction but contracts when light travels through it in the opposite direction. To minimize the influence of thermal fluctuations, several steps can be taken. Insulation and thermal control of the FOG helps reduce the influence of thermal effects. However, these methods have limited effectiveness in applications where space constraints and large temperature fluctuations exist.

Another method to minimize thermal effect is to wind the coil in a symmetric pattern. In symmetric patterns, the effects on one end of the fiber are mirrored onto the other end. Environmental effects shift the two light beams by the same amount so they

remain in phase. Therefore, reciprocity is maintained in a symmetric pattern by winding one end of the fiber close to the mirrored end, so that they experience the same changes.

To wind such a coil, the middle of the fiber must be laid down first. Then successive layers can be wound on top. The fundamental process is pictured in Figure1.6. First, a length of fiber is split between two supply spools, so that the middle of the fiber is exposed. When the active spool winds, the inactive spool becomes fixed and rotates with the product spool. After the active spool winds, the inactive spool becomes active and starts its winding process. These steps are repeated until the symmetric coil is finished.

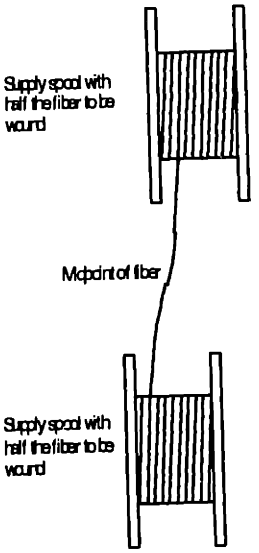

1. Fiber is divided between the two supply spools.

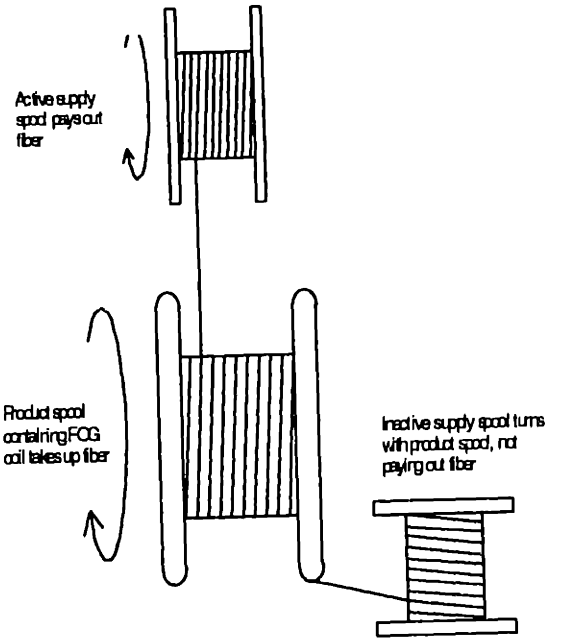

2. One supply spool pays out fiber while the other remains inactive.

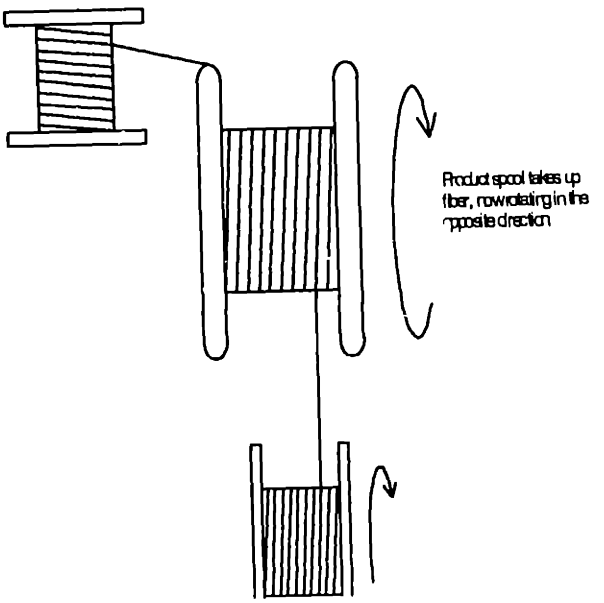

4. The two supply spools alternate paying out fiber until the coil is completed.

Figure 1.6 Symmetric Wind Protocol [Lin].

There are many possible ways to wind a symmetric coil. One popular pattern is the quadrupole. A cross-section of this pattern is shown in Figure 1.7. The white and black shading differentiates the fiber originating from one supply spool from the other. The number on the fiber represents the number of turns from the center of the fiber. Notice that the number of turns from the center, for both the black and white fibers, are in close proximity to each other. This pattern thus resists time varying thermal effects, since both ends of the fiber experience similar effects. Symmetry thus allows for cancellation of thermal effects.

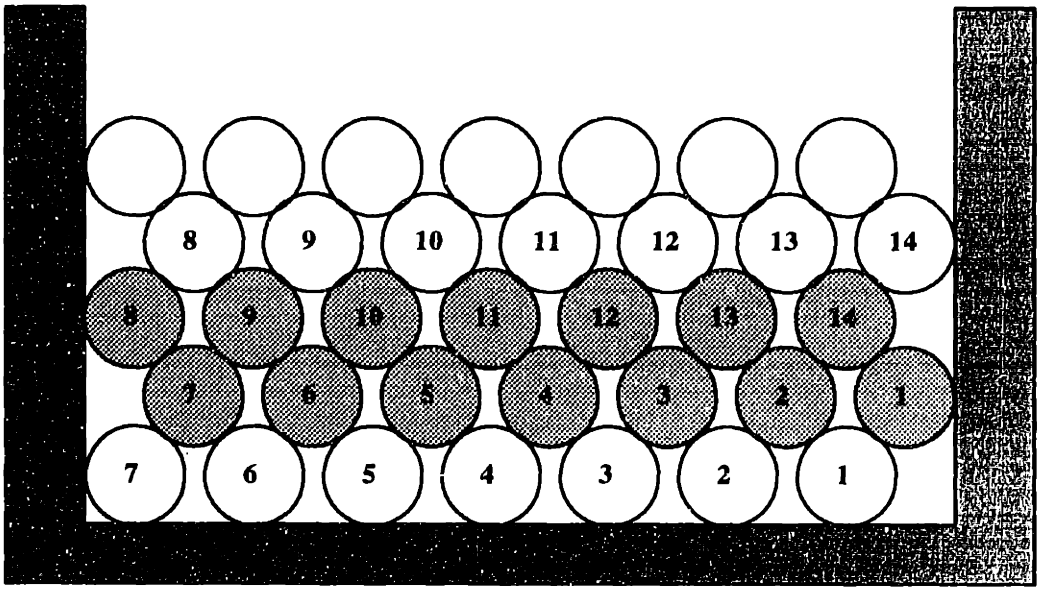

Figure 1.7 Quadrupole Cross Section.

The issues surrounding the FOG coil performance are used to develop the functional requirements for a coil winding machine. To minimize non-reciprocal events such as random polarization effects and thermal effects, the following features are required:

The Machine:

1. Must not physically damage the fiber by nicking or over-bending the fiber.
2. Must control and maintain a low level of tension while winding.
3. Must be capable of winding in an orthocyclic fashion.
4. Must be capable of winding an error free coil. Error is defined as any deviation from the desired winding pattern.
5. Must be able to wind symmetric pattern. The supply spool must be able to rotate with the product spool.

Only by adhering to these guidelines, can a high performance coil be possible.

2 Proposed Coil Winder

2.1 Current Coil Winding Methods

Many of the FOG coils wound today use a semi-automated machine requiring manual intervention. A skilled technician must constantly monitor the progress of the wind. When an error is detected, winding stops and the fiber is guided into place. The technician provides guidance with the assistance of a Teflon tool. This method proves to be inadequate in consistently producing high-grade coils. The technician can not maintain proper spacing between fibers with sufficient accuracy. Without proper spacing of the fiber, the coil cannot absorb the manufacturing variation of the optical fiber. This variation can reach as high as ±10% of the nominal diameter. Manual intervention is also necessary for swapping active and inactive supply spools. This process provides many opportunities for fiber damage.

2.2 Proposed Winder

In 1995, work began on a fully automated fiber optic coil winding machine. The primary goal of the project was to reduce the cost in the production of FOG coils. The development team first created a test bed winder for design validation and testing. A final machine was developed based upon the data obtained from the experimental test bed. This machine met many requirements set forth by the customers. A defining feature of the machine is its flexibility. The machine is able to wind coils of varying patterns, geometric size and tension levels.

In addition to flexibility, the machine is able to achieve a high level of accuracy in terms of fiber placement and tension control. To achieve its primary goal, the winder is designed to have a throughput that is several times higher than conventional manual winding techniques.

2.2.1 Flexibility in Design

The flexibility of the proposed coil winder enables it to wind several different patterns. Most coil winders are built to wind a specific pattern such as the quadrupole pattern. To wind such a configuration, 'a' and 'd' are necessary from Figure 2.1. However, the proposed winder is capable of all four configurations, which increases the possible number of patterns dramatically. The transition from one configuration to the next utilizes a positioning system.

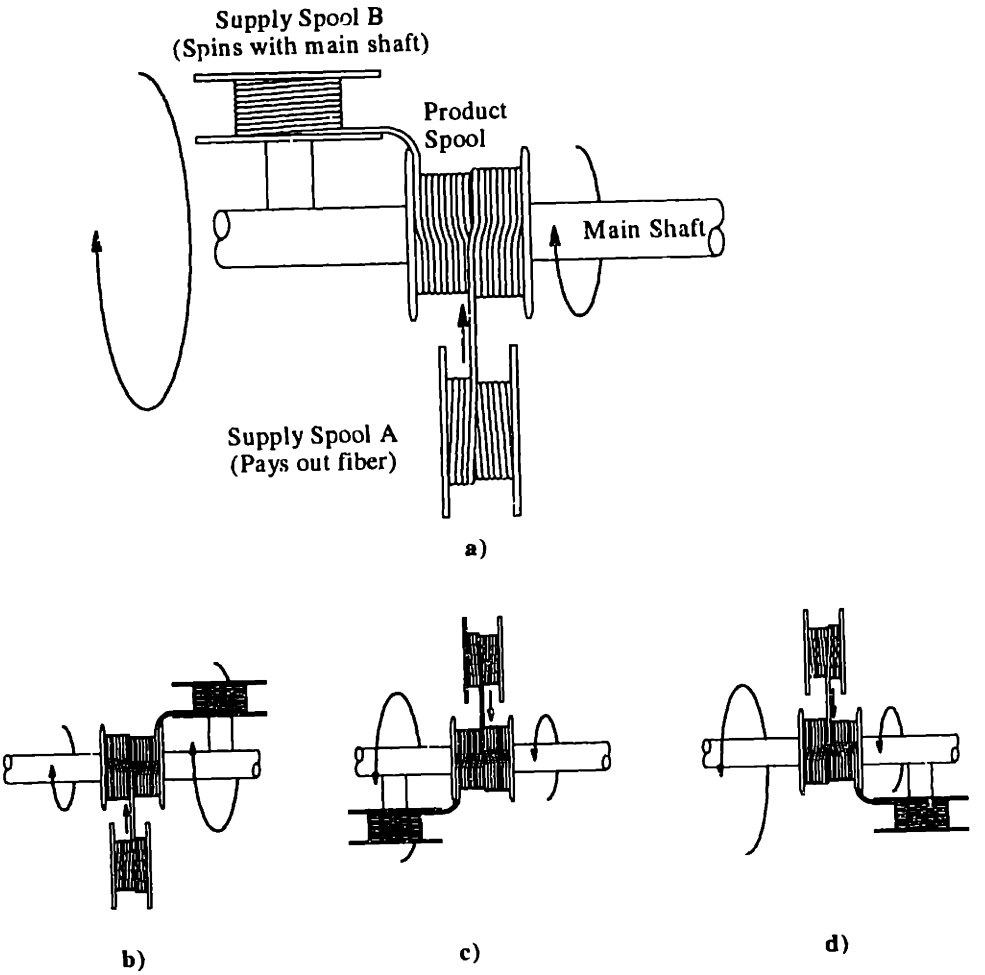

Figure 2.1 Four Configurations Needed to Wind Any Pattern [Lin].

The positioning system is composed of three orthogonal linear stages and two rotary stages. It serves to reposition the supply spool to an active or inactive state. In the active state, the supply unit pays out fiber from the supply spool. In the transition to an inactive state, the positioning system rotates the supply unit until it is adjacent to the main shaft. Then, the ride clamp locks the supply unit to the shaft while the positioning system decouples mechanically and electrically from the supply unit.

2.2.2 Supply Unit and Tension Control

The supply unit subsystem primarily serves to pay out fiber from the supply spool and to control fiber tension. The supply units are portable systems that connect and disconnect to the positioning system or the ride clamps. Figure 2.2 shows a picture of the supply unit. Normally, the fiber is fed off the supply spool, under the dancer pulley, and over the guide wheel. The guide wheel helps position the fiber horizontally onto the product spool. Its thin profile allows it to wind close to the edge of the mandrel without interfering with the flanges.

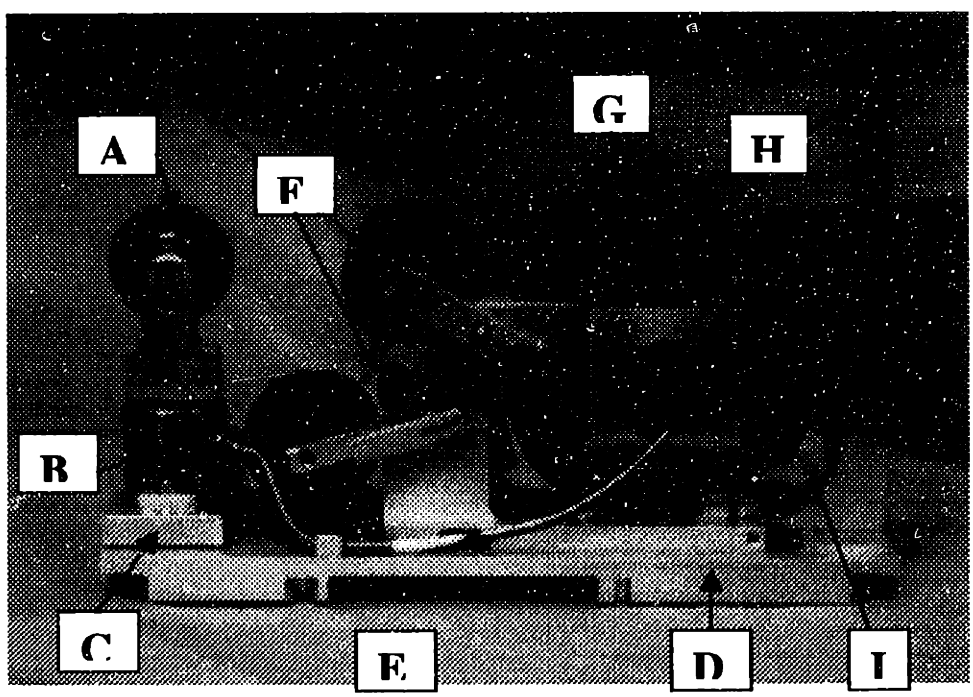

Figure 2.2 Supply Unit. A) Guide Wheel, B) Tension Sensor, C) Guide Wheel Fine Alignment System, D) Base Plate, E) Dancer Pulley, F) Passive Tension Spring, G) Supply Spool, H) Ride Arm, I) Brake [Lin].

Two PID control loops control the payout rate of the fiber and the tension level. The first control loop uses encoder feedback from the dancer to control the output to the supply spool motor. This maintains the dancer in a horizontal position. The supply spool

must lend the same amount of fiber as the amount of fiber wound onto the product spool in order to maintain the dancer's position. In this configuration the fiber experiences a constant tension equal to half the weight of the dancer assembly.

The second control loop maintains the desired fiber tension. Fiber tension level is fedback from the load cell and is used to control the dancer motor. When the tension level is too low, the dancer will push down in order to increase tension, and the opposite occurs when the tension level is too high. A schematic of these two control loops is shown in Figure 2.3.

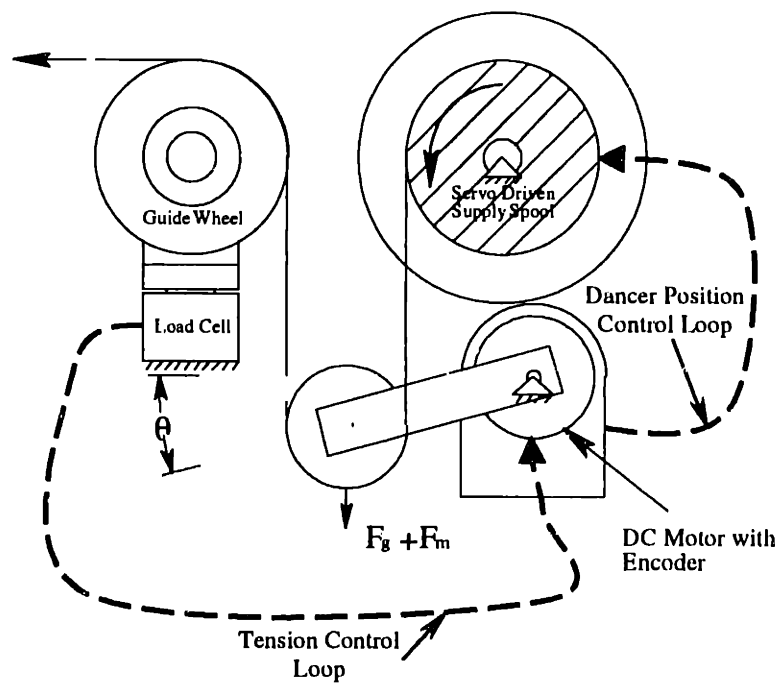

Figure 2.3 Active Dancer Tension Control System [Lin].

The dancer tension control design proves to be superior to its dancerless counterpart. Without a dancer, only one control loop is necessary. The load cell feedback is used to determine the command signal to the supply spool motor. Therefore, one control loop

controls both the payout speed and tension. However, the dancerless design provides good control only with low accelerations and neatly wound supply spools. In contrast, the dancer design provides for more robust control over such disturbances and uncertainties. Experiments have shown that the supply unit can control the tension to within ±0.5 gram of tension.

The supply units also provide a means to store the supply spool while it is inactive. The inactive state is referred to as the ride position. To maintain tension in the ride position, the dancer is biased against a spring element. Then, the brake locks the supply spool in place. The spring applies 20 grams of tension so that tension is not lost when the dancer's weight vector changes direction as the supply unit rotates.

2.2.3 User Interface

To control the MIT winder the design team also developed a machine interface. Flexibility is also built into the interface in the form of a command interpreter. After a new winding pattern is conceived, a customized sequence of commands can be developed. An operator can accommodate for uncertainties by altering a list of commands. Commands can be grouped into two categories, execution and parameter commands. Execution commands provide actuation cues to the motors and stages, while parameter commands modify the winding parameters.

A list can also be called within your command list. A sublist can be reused for situations that occur regularly, such as swapping the supply unit to its different states. The execution of the command list operates in a fully automated mode where commands

execute continuously, one after another, or in single mode where one command is executed individually.

The command list allows for a flexible and quick means of process development in the manufacturing of FOG coils. The winding routines can be customized, developed, tested, and optimized without having to modify the software code.

3 New Machine

In 1996, a customer commissioned the MIT/MI to develop a second generation automated fiber optic gyroscope coil winder capable of winding strategic grade coils. MIT/MI worked with the customer to develop a list of target specifications to meet the customer's goals.

The design and research from the first MIT/MI winder formed the foundation for the new winder. The previous design satisfied some of the new target specifications, but additional research and development including the area of tension control was needed. The new specifications required higher accuracy and a broader range of possible tension values for the tension control system. In addition, the customer desired active tension control during all winding stages. This involved the modification of the existing ride tension mechanism, which applies tension using a spring element. To meet the new specifications, modification to the supply unit and the addition of an active ride system needed development.

Apart from the supply unit, two other subsystems were modified. To improve the accuracy in fiber positioning, the critical axis of the positioning system needed to be identified. Consequently, the winding accuracy was found to be most sensitive to the x-axis since this axis controls the horizontal location of the fiber being wound. The original design uses a rotary encoder to sense the x position. This method is more prone to errors resulting from backlash. As a replacement, a more accurate linear encoder system was installed on the x stage instead.

The second subsystem was the ride clamp. The previous design functioned smoothly, but required an air pressure supply. Unfortunately, this was not readily

available in the clean room designated for the new winder. Thus, new ride clamps were designed to operate using D.C. motors instead of pneumatic pistons. A detailed discussion of the ride clamp design can be found in [Darley]. The actuation of the ride clamps was achieved through the D.C. Motor, in conjunction with a lead screw and nut assembly. Attached to the nut is an aluminum backing plate that provides two clamping surfaces. The other clamping surface of the quasi-kinematic coupling is fixed with respect to the lead screw. This design has been shown to provide 20 times the minimum clamping force needed to hold the supply unit in place during winding.

3.1 Supply Unit Redesign

The basic layout of the supply unit remained in tact, but two changes were implemented. First, a counterbalance was introduced to the dancer arm. Gravitational disturbance can cause tension to fluctuate ±2.5 grams in the previous dancer design. In addition to gravity, centripetal acceleration of the dancer mass can also contribute to the tension. At 0.5 revolutions/sec, centripetal acceleration increases tension level by 1.5 grams. The addition of a counterbalance eliminated the disturbances caused by both gravity and centripetal acceleration.

In the design of the new counterbalanced dancer, geometric constraints was one of the design issues that required resolution. A limited amount of space was available for the counterbalance. Extending beyond this region would result in collision with the other supply unit. It was important that the dancer was free to move through a given range. The counter balance must also have the capability for fine adjustments. This will be conducive to a more accurately balanced dancer arm.

With the requirements above in mind, two designs were considered. The first incorporated a slotted mass fixed to the dancer via a mounting screw. Adjustments to the balancing mass were made by loosening the screw and shifting the position of the mass. The second design shown in Figure 3.1 uses a cylindrical mass that screws onto a finely threaded rod. The second design was chosen for its compact configuration and its capability for fine adjustments. With this in place, rotation of the supply unit resulted in negligible change in dancer orientation. Acceleration or gravity does not affect the counterbalanced dancer.

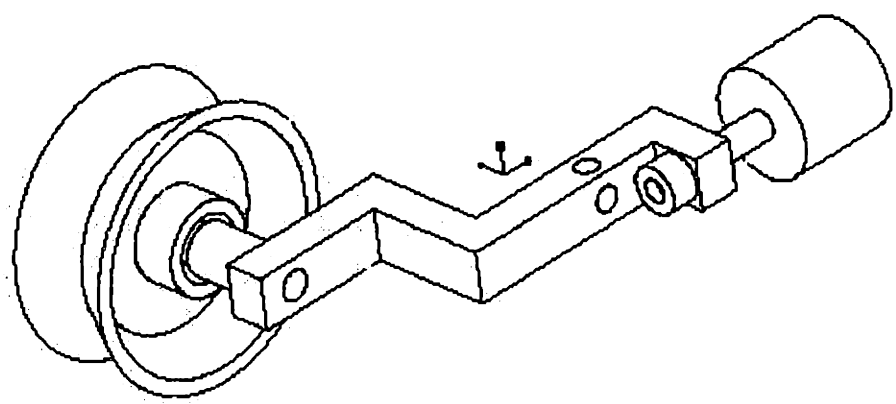

Figure 3.1 Counterbalanced Dancer Arm.

Once the counterbalance was incorporated, tension contributed by the dancer's mass was now eliminated. Therefore the dancer motor alone needed to provide all of the

desired tension. This led to the second modification of the supply unit. A new motor capable of meeting the customer's requirements was selected and installed. This motor has more torque than the previous dancer motor, but had to be kept within certain dimensional parameters to avoid interference.

3.2 Active Ride System

To actively control tension in the ride position, power and signal connections must reach the rotating supply unit. The active ride system was designed for this purpose. The system consists of two parts. In order to provide electrical connections along a rotating shaft, instrumentation-grade slip rings were selected. For each channel, the slip ring has a wiper and ring pair that stays in contact during rotation. The ring then transfers the electrical signals to the ride clamp.

The electrical connection between the ride clamp and supply unit were established using a double sided PCB board and spring contact probes. Mounted to the ride clamps, the PCB board features vertical copper lines that come into contact with the supply unit's probes. The vertical contacts allow the supply unit to clamp at different heights relative to the ride clamps. The change in height is due to the gradual increase in coil thickness as the coil is being wound. Further detail of the active ride system is found in [Darley].

3.3 Electrical and Software enhancements

Along with the mechanical modifications, Electrical and software enhancements were also needed. Each ride clamp has the capacity to hold only one supply unit at a time.

When a supply unit is in the ride position it must be connected to its own corresponding electrical connection. There are two main reasons why the supply units must be connected to their own electrical connection. First, the load cell of each supply unit has a calibrated thermal compensator that operates correctly only if connected to the proper load cell. Secondly, the controller gains are specifically tuned to each supply unit to achieve the best possible performance. Therefore, by connecting the supply unit to the wrong electrical connection inferior performance will result. A system that allows switching of electrical connections is shown in Figure 3.2.

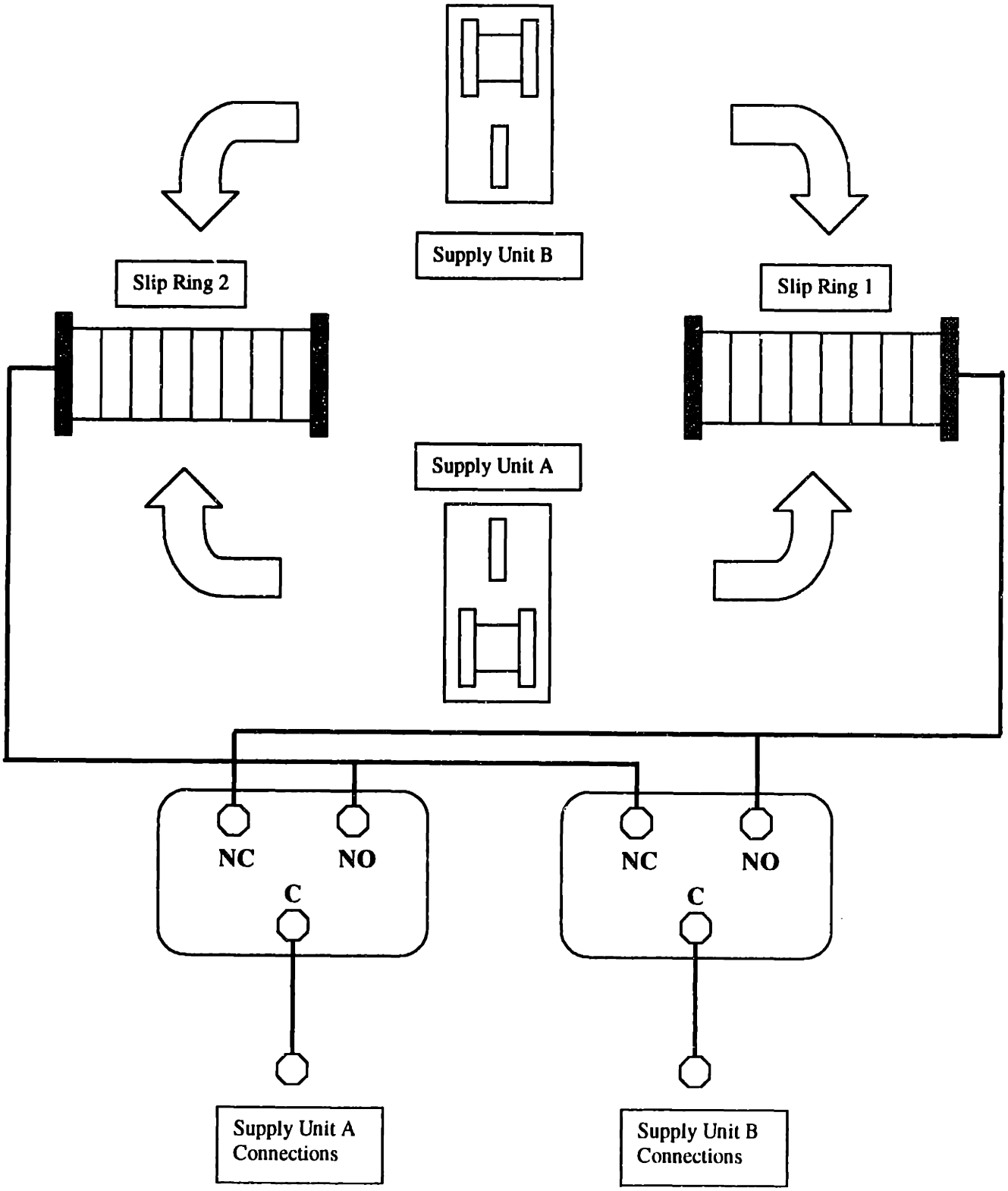

Figure 3.2 Active Ride Switching Connection System.

The wires shown in the schematic represent 16 signal channels that are essential for tension control in the ride position. Each relay consists of four single-pole double-throw relays. This means that activation of the relay switches eight channels at a time. Normally slip rings one and two are connected to supply unit A and supply units B's controls respectively. Once activated, both relays switch at the same time so that the supply units remain connected to their respective control signals.

Electrical modifications were also made to the supply unit detection system. It was imperative that the machine be capable of monitoring its own status. All the servo-controlled motors use encoder feedback to extract their positional state. This information is useful in preventing collisions. The machine code will not execute a move that would result in interference. In addition to the stage locations, it is also important to know the location of the supply units. The previous design used infrared proximity sensors to check for the presence of the ride arm of the supply unit. This method was used for detection in the ride position only. Unfortunately, the sensors can only be used when the supply unit is in an upright orientation and at rest.

A more reliable method for supply unit detection in the ride position is to use an electrical connection. A schematic of the new detection system is shown in Figure 3.3. The system utilizes the extra channels available on the slip rings to connect to the digital input terminals. Once the supply unit is clamped, the jumper located on the supply unit shorts the digital input to ground. By checking the digital input channel, the presence of the supply unit is known. This system thus serves as a reliable detection method for any orientation of the clamped supply unit.

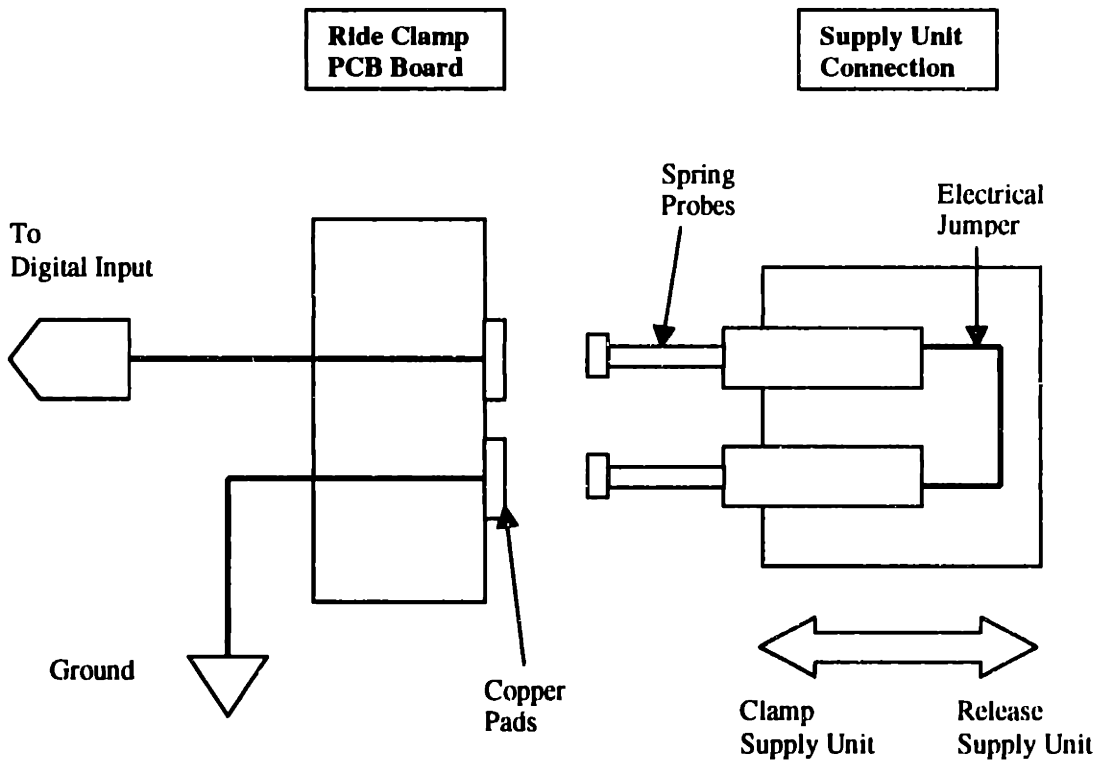

Figure 3.3 Supply Unit Detection Circuit.

Another electrical issue involved the relays used for the machine. When the winder is turned on, the digital IO control card initializes. During initialization, the DIOs, which are used to control the relays, switch to a high state for a split second. This quick flash of the DIOs in turns activates the relays for a short period. Although this causes no apparent damage, the relays controlling the z-axis brake release temporarily, allowing the position system to slip. Since this movement of the z-axis is not accounted for by the winder, position data for the z-axis will be incorrect. To correct for the error, homing of the z axis is needed whenever the winder program is executed. This is not desirable if the machine is concurrently winding a coil. Since the initial DIO flash cannot be eliminated, discharging the relay is the next option. The winder program was given a new clean-up procedure which first cuts the power to the relay board. A pair of unused

relays is then activated for a few seconds to discharge the board. After the relay board has been discharged, the quick DIO flash cannot affect the relays.

3.4 Tension Control States

With the hardware and electrical systems in place, the last necessary component is the software needed to drive the machine. The winder program has four primary tension control modes: 'OFF', 'PASSIVE', 'ACTIVE' and 'RIDE'. In 'OFF' tension mode, the brake is engaged and the dancer motor is disabled. While this mode worked well for the previous winder, the current counterbalanced dancer will lose tension when the dancer is turned off. Tension loss may lead to loosening of the fiber or unwinding of the coil. To maintain tension in the 'OFF' state a small motor bias is applied to the dancer, instead of disabling it.

To change from the 'OFF' state to 'PASSIVE' mode, the brake releases the supply spool which then pulls back with a calibrated motor bias. This action raises the dancer arm until it comes in contact with the spring probe. This mode is used in situations that do not require accurate tension control, yet still involves fiber moving in or out of the supply unit. For example, unwinding and supply unit swapping are situations where accurate tension control is not critical.

Active tension control is necessary while winding onto the product coil. The active supply unit winds using the active tension mode. With servo control, the supply spool lowers the dancer until it becomes horizontal. Then the load cell dancer motor loop engages and begins to control tension levels.

The final control state is the ride mode. Before the payout clamp disengages from the supply unit, the supply spool pulls the dancer up against the spring probe with 20 grams of tension. Then the brake is engaged to maintain tension.

Two additional control states are added to enable active tension control in the ride position. First, the 'Ride Prep' mode lowers the dancer to a horizontal position and engages the brake. This transitional mode moves the dancer away from the spring so that only the dancer motor is in control of the tension. The brake is engaged because fiber payout is not needed in the ride position.

The second state is the 'Ride Active' mode. A calibrated motor bias is applied to the dancer and tension is maintained during rotation. In this mode low tension levels can be maintained with a reasonable amount of accuracy.

3.5 Ride Tension Control

To actively control tension, feedback from the load cell is needed. The same is true for active tension control in the ride position. It is difficult to obtain accurate tension data from a supply unit in the ride position. While the supply unit rotates, the guide wheel assembly siting on top of the load cell changes the load cell readings. Deviation from the actual tension levels depend on the supply unit's orientation and rotational speed. Load cell data without fiber is shown in Figure 3.4. As the supply unit rotates, the orientation of the supply unit causes the tension to vary sinusoidally. At slow speed, the orientation is the most dominant factor. However, as the rotational rate increases, the centripetal acceleration becomes a more significant factor than before.

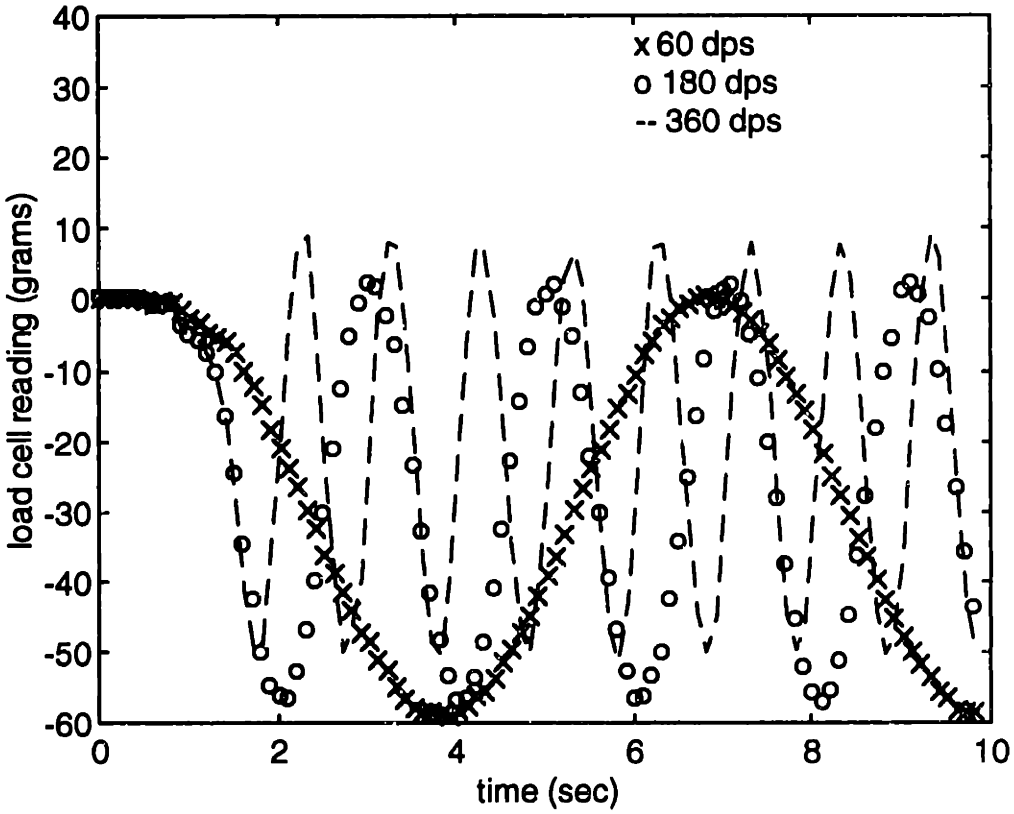

Figure 3.4 Load Cell Reading at Varying Windings Speeds.

Ideally if the orientation and rotational velocity data of the supply unit are available, the load cell data deviation can be eliminated. Two terms are needed to compensate for the load cell error caused by the guide wheel assembly mass. The first term shown in equation (4) accounts for the vertical component of the assembly's mass. The second term , which is proportional to velocity squared, accounts for the force applied by centripetal acceleration of the mass. The following equation shows the compensation factor subtracted from the load cell reading to get a more accurate reading of the actual fiber tension.

$$F_{comp} = m(Cos\theta - 1) + cw^2 \quad (4)$$

where,

theta = Supply unit rotational orientation.

w = Supply unit rotational velocity.

m = Mass of the guide wheel assembly.

c = constant

Values for m and c are 30.6grams and 6.57e-5 grams/dps^2 respectively. With compensation, the resulting load cell data is shown in Figure 3.5. For this experiment the supply unit is rotated at 60 degrees/sec (dps) and then at 270 dps.

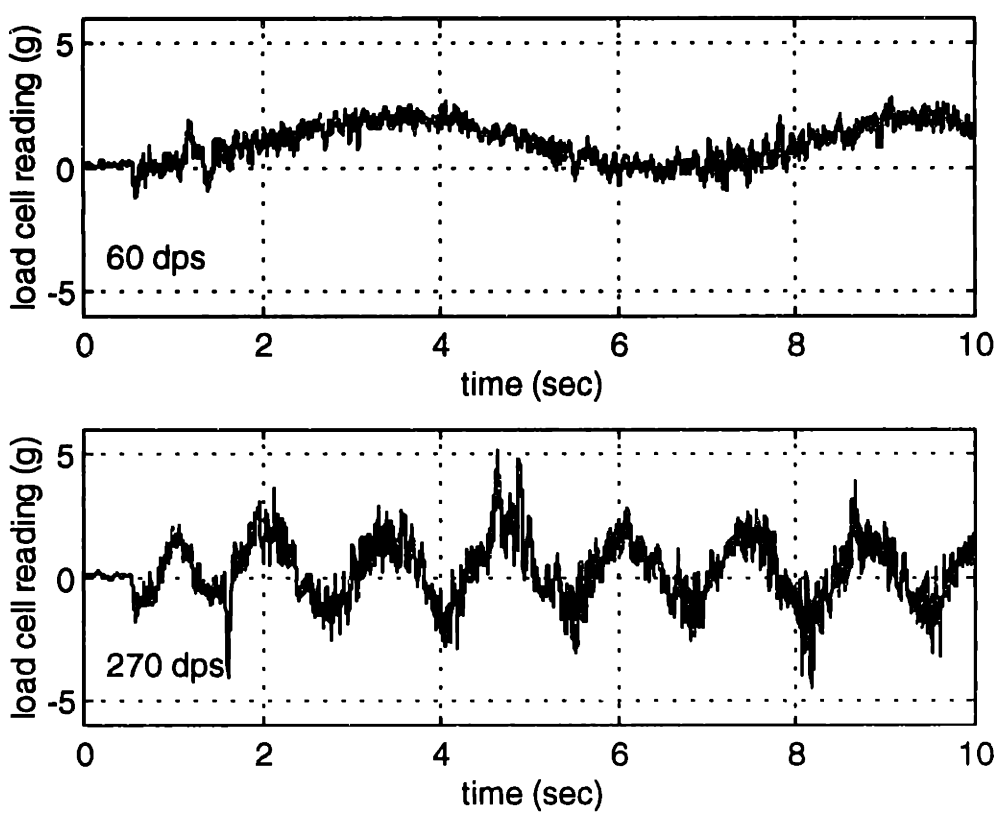

Figure 3.5 Load Cell Reading with Initial Compensation Factor. Top: At 60dps. Bottom: At 270 dps.

Compensation reduces the load cell and tension level discrepancy to within ±5grams for 270dps and ±2.5 grams at 60dps. The results indicate that load cell data errors fluctuate with respect to position and increase in magnitude as the velocity increases. Therefore a third term, proportional to position and velocity, should help reduce the deviation further. The new compensation factor is derived and is shown in the equation below,

$$F_{comp} = m(Cos\theta - 1) + cw^2 + kwCos\left(\theta + \frac{\pi}{4}\right) \tag{5}$$

where,

k = constant = 0.007

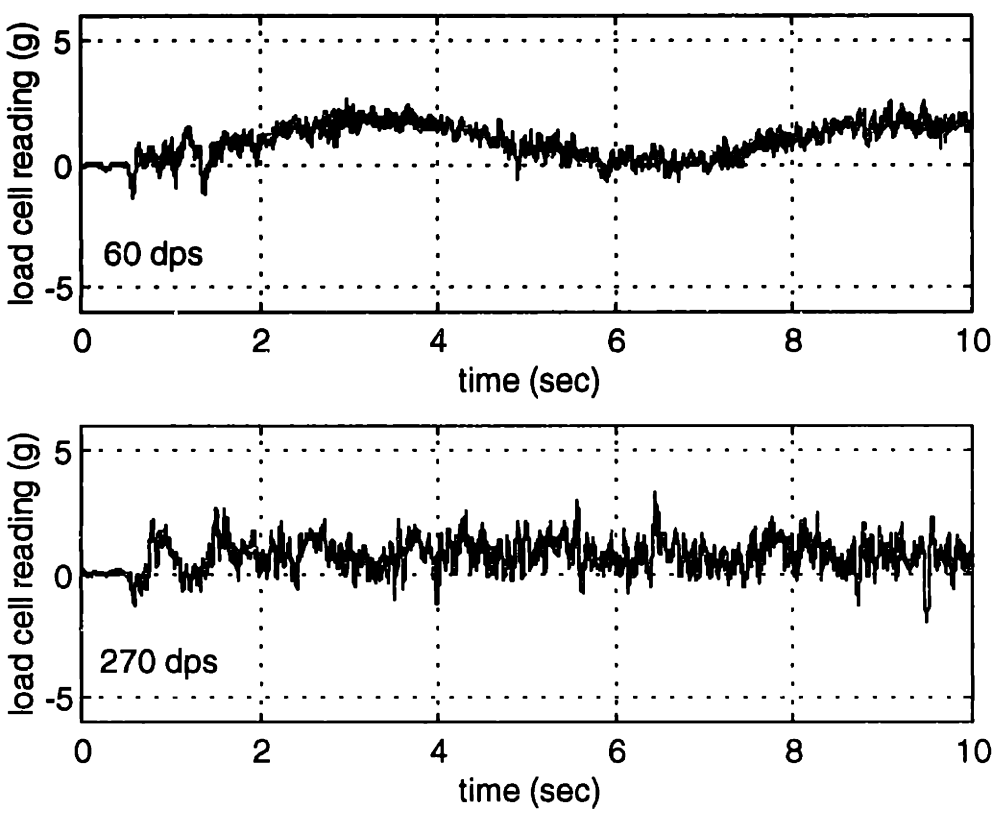

Figure 3.6 Load Cell Reading with New Compensation Factor. Top: At 60dps. Bottom: At 270 dps.

Even with the additional compensation, the error and noise levels in the load cell signal discourages the feasibility of active ride tension control. Another approach to ride tension control is to use an open loop control. By calibrating the dancer motor with the load cell readings, the dancer can apply tension close to the desired tension levels. To characterize the performance of the open loop control system, repeatability and accuracy experiments were performed on the actual winder. These experiments were performed with the supply units in a stationary state. Similar performance results with the supply unit spinning should be possible if the dancer arm is perfectly balanced. In both experiments, the dancer motor is turned off before each trial to simulate the transition to 'Ride Active' tension control mode. Figure 3.7 and Figure 3.8 show the results of the repeatability and accuracy of the open loop control scheme. With open loop compensation tension control does exhibit good repeatability with only ± 0.1 gram of variation.

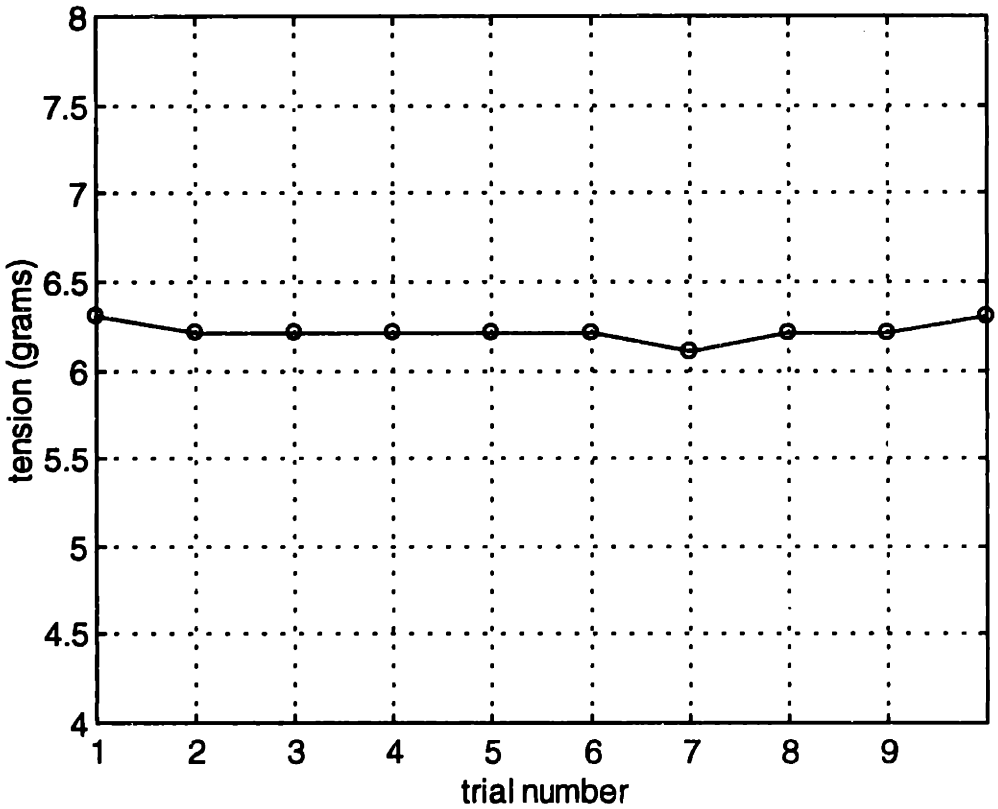

Figure 3.7 Open Loop Control Repeatability Experimental Results.

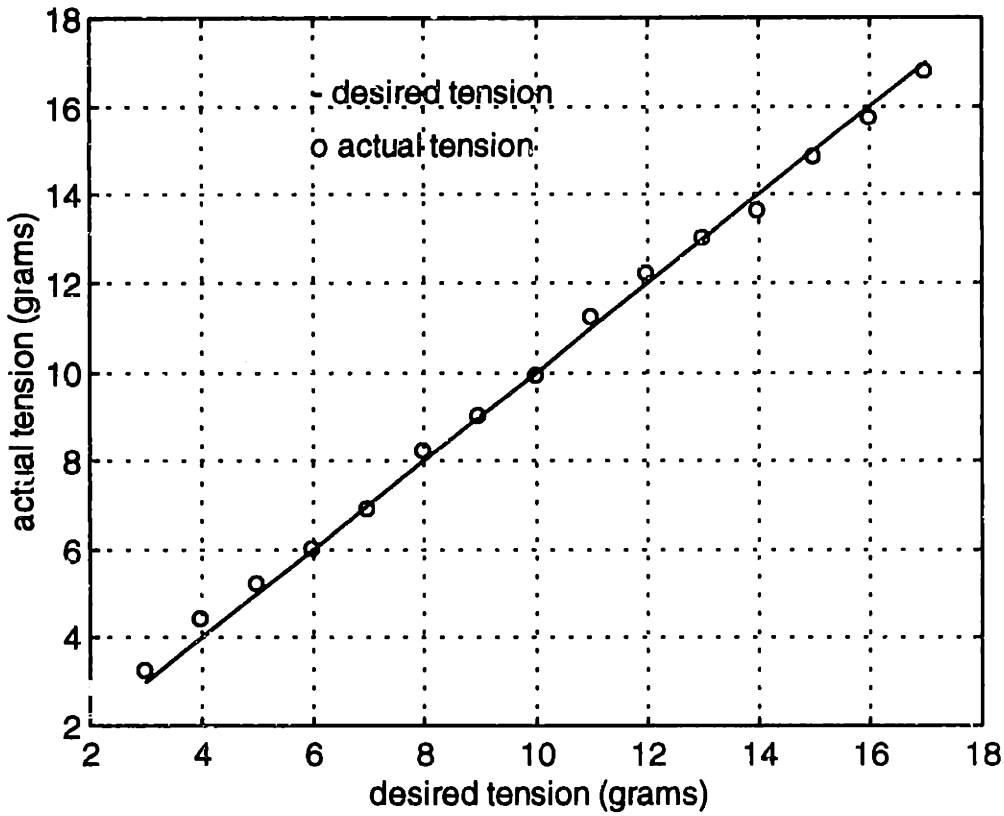

Figure 3.8 Open Loop Control Accuracy Experimental Results.

The open loop accuracy experiment was performed in a similar fashion to the repeatability experiment. However, the desired tension was increased by 1 gram for each trial. The results show a close correlation between the desired tension and the actual tension acquired. Accuracy was always maintained to within ±0.4 gram of tension.

Although "classical" active tension control is not implemented on the winder in the ride position, the new system does allow lower tension levels in the ride position. The open loop control scheme is able to achieve a fair amount of accuracy for a large range of tension and proves to be repeatable in test. Furthermore, since the fiber in the ride position is not being wound onto the coil, small fluctuations in tension will have little impact on the performance of the final coil.

4 Active Tension Control

During FOG coil production, it is important that the fiber be wound at low tension levels. The performance of a FOG degrades when high stress levels in the fiber cause bifringence and attenuation. It is desirable to minimize mechanically induced error by keeping tension levels and transient errors low.

The customer's requirements defined two characteristics that are desirable for a tension control system: good steady state and transient response. The control system should be able to achieve good steady state response. After an initial tension change the response should dampen out and converge close to the desired tension level. In addition to steady state, the transient response is also important. Systems with good transient response can change tension levels quickly and reject external disturbances. At current winding speeds fiber dynamics are too fast to be of real importance, since fast tension transients are averaged out when winding at relatively slow speeds. The transient response of the system depends more heavily on the time constants of the control system.

With the above two performance characteristics in mind, the tension control system of the winder was examined and characterized. A model of the tension control system was created in order to study the general dynamics of the system. Then, the model is used to investigate the effectiveness of an alternative control method. The final section of this chapter will present and discuss the experimental results.

4.1 Simulation

In order to better understand the dynamic response and tension control capabilities of the tension control system, a model of the system was developed. A schematic of the tension control system is shown in Figure 2.3. From this schematic an idealized-lumped parameter model was produced (Figure 4.1). Notice that the model represents the optical fiber as compliant members, although a typical glass fiber has a modulus of elasticity of 75 GPa and can be considered stiff. The compliance does not represent the longitudinal stiffness of the fiber, but rather the bending stiffness. The bending stiffness causes the fiber to resist the formation of small radius bends. Consequently the fibers act as low stiffness springs until enough force is applied to make them tight.

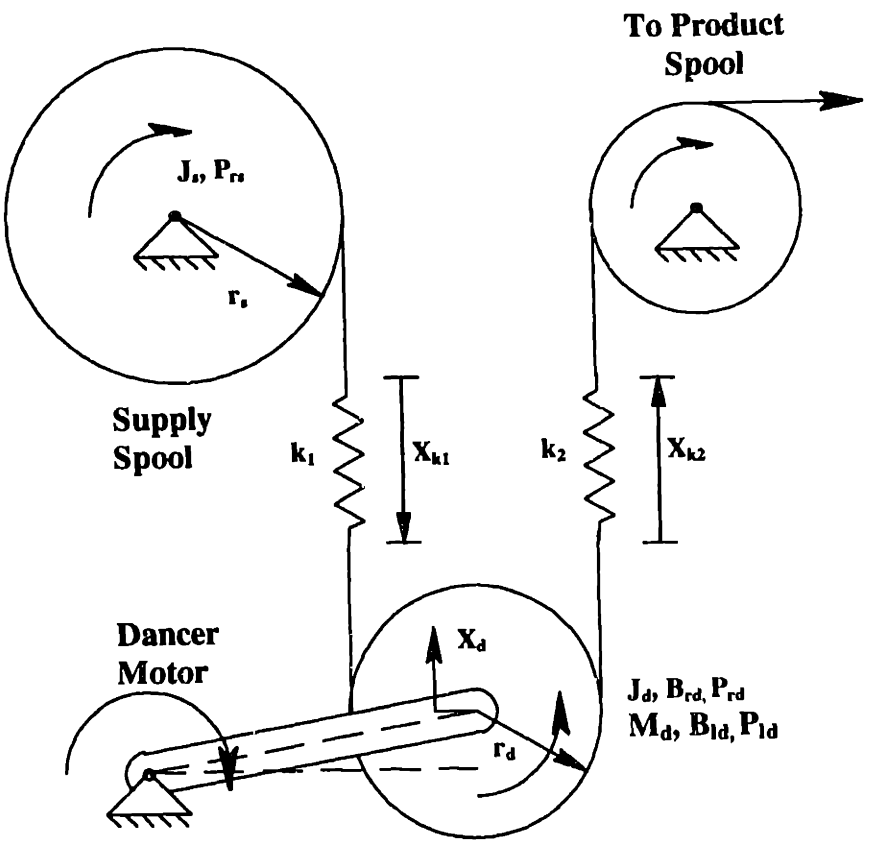

Figure 4.1 Lump-Parameter Model of the Active Dancer Control System.

Where,

J_s = Moment of inertia for the supply spool assembly.

J_d = Moment of inertia for of the dancer pulley assembly.

M_d = Mass of the dancer arm assembly.

B_{rs} = Rotational viscous friction of the supply spool assembly.

B_{rd} = Rotational viscous friction of the dancer pulley assembly.

B_{ld} = Viscous friction of the supply dancer motor.

P_{rs} = Rotational momentum of the supply spool assembly.

P_{rd} = Rotational momentum of the dancer pulley assembly.

P_{ld} = Linear momentum of the dancer arm assembly.

X_d = Displacement of the dancer pulley.

X_{k1} = Displacement of spring element K1.

X_{k2} = Displacement of spring element K2.

r_s = Radius of the supply spool.

r_d = Radius of the dancer pulley.

The following assumptions are used to develop this model:

- Fiber weight is negligible.
- Fiber is compliant.
- Fiber segment between guide wheel and product spool is short. Therefore, the fiber segment can be considered stiff.
- Dancer pulley moves vertically for small angles.
- Product spool acts as a velocity input (flow source).
- Supply spool motor acts as a torque source (effort source).
- Dancer motor also acts as a torque source (effort source).
- Guide wheel inertia and friction are negligible.

4.1.1 Bond Graph

In energy-based modeling, a graphical model can be developed to represent how elements within the system interact and exchange energy. Energy-based modeling consists of three distinct elements: energy sources and sinks (S), energy storage elements (I, C) and energy dissapative elements (R). These elements are connected at junction structures where energy is conserved. Two types of junction structures are the common 'effort' junction (O) and the common 'flow' junction (1). The bond or line connecting the elements to a junction represents an exchange of power between the two elements connected. For more detail on bond graphs and energy-based modeling, refer to [Karnopp, et al]. Using energy-based modeling techniques, a bond graph of the lumped-parameter model is developed. The bond graph is shown in Figure 4.2.

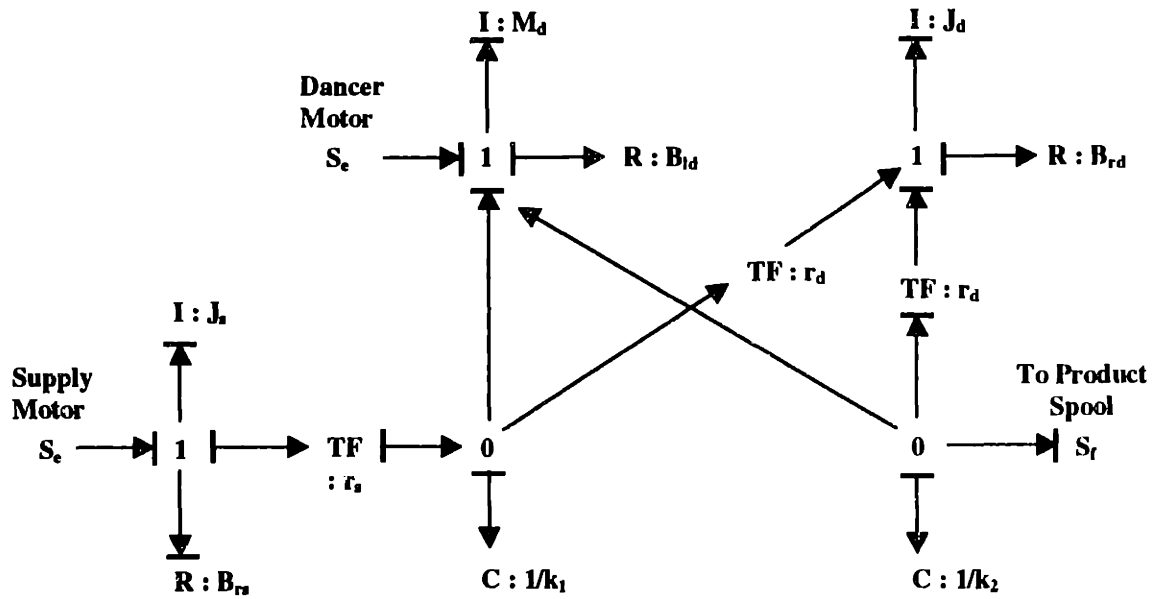

Figure 4.2 Bond Graph of Active Dancer Control System.

A 5th order system is derived from the bond graph developed. For this system, five independent state variables are selected. The five state variables are the following:

the displacements of two spring elements X_{k1} and X_{k2}, the rotational momentum of the supply spool P_{rs} and the dancer P_{rd}, and finally the linear momentum of the dancer mass P_{ld}. With the bond graph and the chosen state variables, a state space representation is derived.

State Space Equations:

$$\mathbf{X' = A[X]+B[U]}$$

$$\mathbf{Y = C[X] + D[U]}$$

Where,

State Variables:

$\mathbf{X} = [P_{rs}\ P_{rd}\ P_{ld}\ X_{k1}\ X_{k2}]$

P_{rs} = Rotational momentum of the supply spool assembly.

P_{rd} = Rotational momentum of the dancer pulley assembly.

P_{ld} = Linear momentum of the dancer arm assembly.

X_{k1} = Displacement of spring element K1.

X_{k2} = Displacement of spring element K2.

Inputs:

$\mathbf{U}$ = [Es Ed Fp]

Es = Torque of supply spool motor.

Ed = Applied force of the dancer motor.

Fp = Linear velocity of the product spool.

Outputs:

Y = [Tf Vd]

Tf = Fiber tension.

Vd = Dancer's vertical linear velocity.

$$\mathbf{A} = \begin{bmatrix} -R_3/I_2 & 0 & 0 & -r_s/C_6 & 0 \\ 0 & -R_{10}/I_9 & 0 & 1/C_6 & -1/C_{19} \\ 0 & 0 & -R_{15}/I_{14} & r_d/C_6 & r_d/C_{19} \\ r_s/I_2 & -1/I_9 & -r_d/I_{14} & 0 & 0 \\ 0 & 1/I_9 & -r_d/I_{14} & 0 & 0 \end{bmatrix}$$

$$\mathbf{B} = \begin{bmatrix} 1 & 0 & 0 \\ 0 & 1 & 0 \\ 0 & 0 & 0 \\ 0 & 0 & 0 \\ 0 & 0 & -1 \end{bmatrix}$$

$$\mathbf{C} = \begin{bmatrix} 0 & 0 & 0 & -1/C_6 & 0 \\ 0 & 1/I_9 & 0 & 0 & 0 \end{bmatrix}$$

$$\mathbf{D} = \begin{bmatrix} 0 & 0 & 0 \\ 0 & 0 & 0 \end{bmatrix}$$

4.1.2 Simulink Model

The state space represents only the mechanical dynamics of the tension control system. A Matlab™ Simulink™ model was developed to simulate the complete tension control system. A schematic of the model is shown in Figure 4.3.

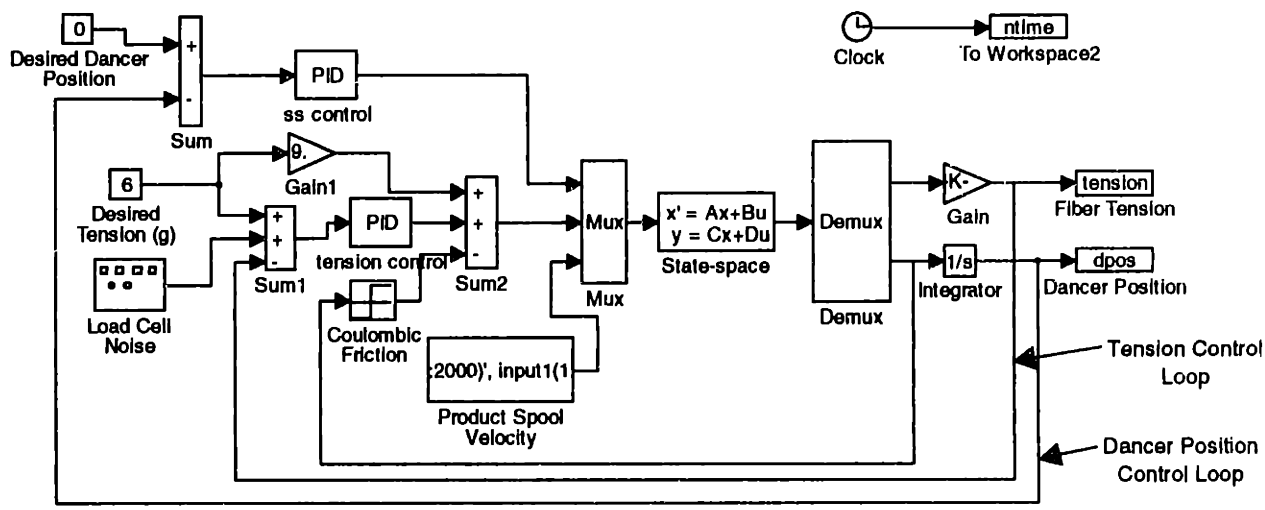

Figure 4.3 Simulink Diagram of Tension Control System with PID control.

The controls are implemented through the two PID control loops. The supply spool motor uses the dancer position as feedback. This loop tries to maintain a horizontal dancer position of zero at all times. The second loop, the tension control loop, tries to maintain the desired tension level of 6 grams with open loop control. This method multiplies the desired tension by the block entitled "Gain 1" in order to achieve the goal.

However, a PID loop with feedback from the load cell is needed to obtain the required accuracy.

In addition to the control loops, two elements are also included to reflect the real physical system with greater fidelity. First, a broadband noise source with a peak of 0.3 grams is added to the tension feedback. This noise represents electrical interference and mechanical vibrations that may influence the load cell signal. The second element is coulomb friction which is added to the dancer motor output. A larger motor is used to attain the customer's requested tension range. One disadvantage of the new motor is the amount of static friction between the motor's commutator and brushes. Coulomb friction is added to the model to account for the dry friction of the dancer motor,.

The parameter values for the simulink model use estimations of the real physical values. The parameters and their approximations are shown below.

$J_s = 9e\text{-}5\ kgm^2$	$M_d = 0.024\ kg$
$J_d = 1.6e\text{-}6\ kgm^2$	$L = 1.375\ in$
$B_{ld} = .001\ Ns/m$	$r_s = .81\ in$
$B_{rs} = .0002\ Nms$	$r_d = 0.5\ in$
$B_{rd} = .0002\ Nms$	$k = 12.57\ N/m$

4.1.3 Simulation results

The Simulink model simulations represent typical winding situations. The product spool speed functions as the only input or external disturbance to the control system. In order to simulate a wind, the product spool remains at rest for one second and

then accelerates to a constant winding speed and maintains this velocity for the rest of the simulation. In situations where high winding speeds are necessary for faster throughput, a velocity profile exhibiting a "slow zone" is used instead. The slow zone decelerates the winding velocity to a slow speed when entering the jog zone. After leaving the jog zone, the winding speed accelerates back up to the regular winding speed. Slowing the velocity allows the guide wheel place the fiber into its designated position more accurately [Lin].

For both the constant speed and slow zone winding profiles, the acceleration and deceleration values are limited to 480 degrees/second^2. The winding and slow zone speeds used are 90 degrees/second (dps) and 30 dps respectively. The same PID control gains are used for all simulations. The gains are tuned in order to achieve accurate tension control without becoming unstable.

Figure 4.4 shows the first group of results. This run simulates a constant winding scenario without load cell noise or coulomb friction in the dancer motor. The simulation shows that at constant winding speed the control system can maintain tension close to the desired level. The only fluctuation occurs when the product spool accelerates from rest. At this point, the supply spool motor cannot accelerate the supply spool in time to keep the dancer horizontal. Consequently, more fiber leaves the dancer loop than enters, causing the fiber to pull up on the dancer. The bottom plot shows that the fiber pulling up against the dancer causes the tension to increase slightly.

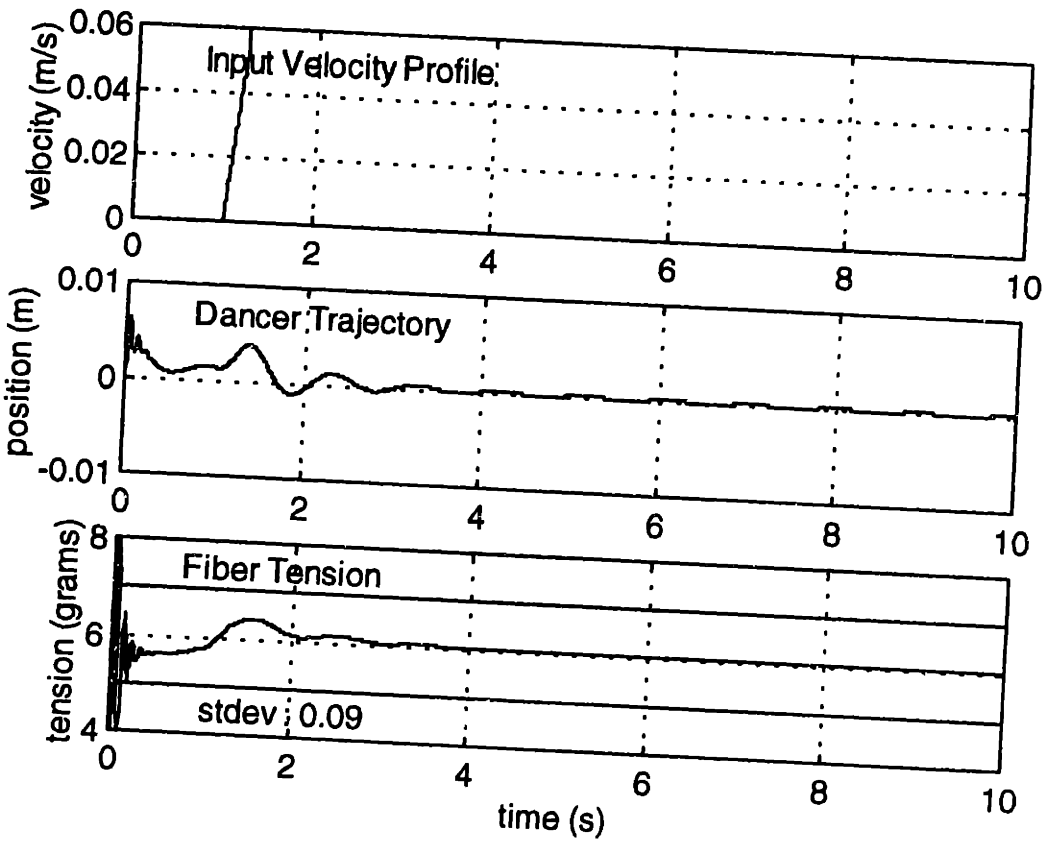

Figure 4.4 Winding Simulation with Constant Speed.

The following figure 4.5 applies a winding profile with a slow zone. Initially, the response mimics that of the previous simulation as expected. However, more transients are apparent during the slow zone's deceleration and acceleration. During the initial deceleration of the product spool, the supply spool continues to pay out fiber at the same rate. This causes both the dancer and tension to drop a bit. As the position error increases, the supply spool begins to pull the dancer to its desired horizontal position. As the product spool accelerates back to the nominal winding speed, a response similar to the initial acceleration occurs. In general, the tension response lags the dancer response. This shows that tension transients are dependent on the response time of the dancer's

position control loop. To improve control, both the inertias of the supply spool assembly and dancer should be minimized.

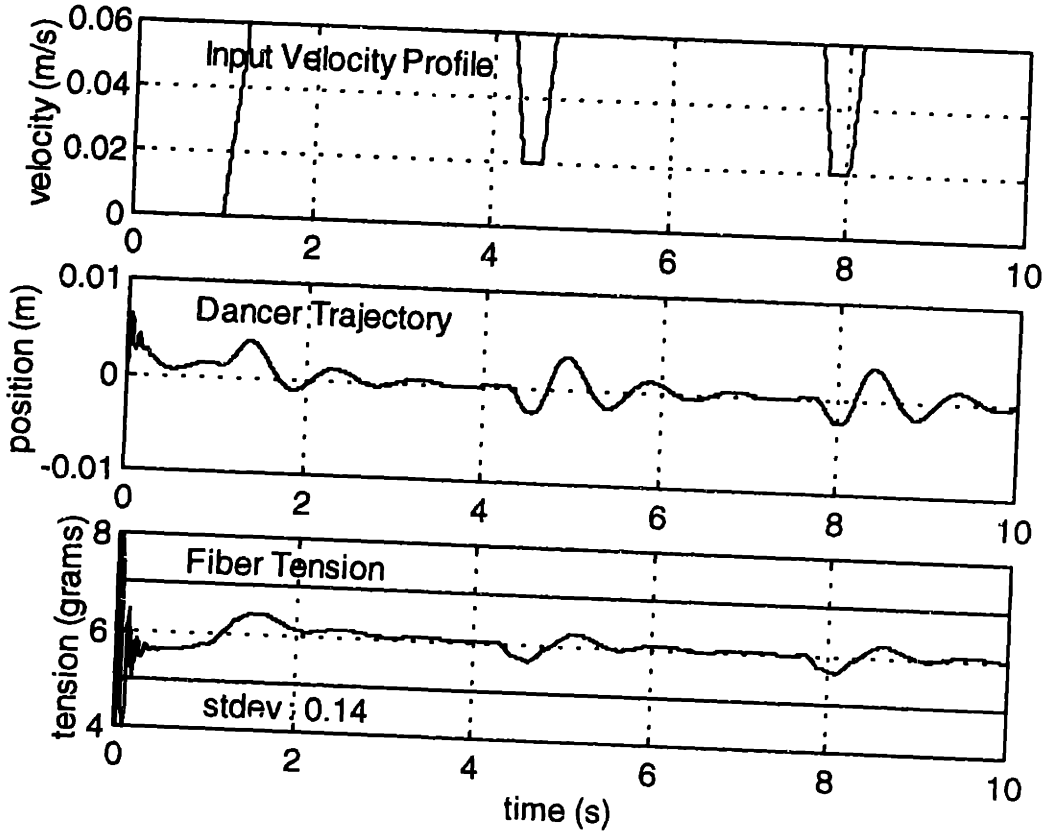

Figure 4.5 Winding Simulation with Slow Zone.

The third simulation introduces broadband noise into the tension control system. Noise is represented in the Simulink diagram by a white noise source labeled "Load Cell Noise." The noise becomes part of the error signal, which is used to calculate the command signal of the dancer motor. The effects of noise are evident in the dancer's position response shown in Figure 4.6. Since the dancer's positional fluctuations directly affect the tension, the noise also causes the tension to fluctuate. The standard deviation for tension increased from 0.14 gram without noise to 0.19 gram with noise. The response indicates the importance of a clean feedback signal.

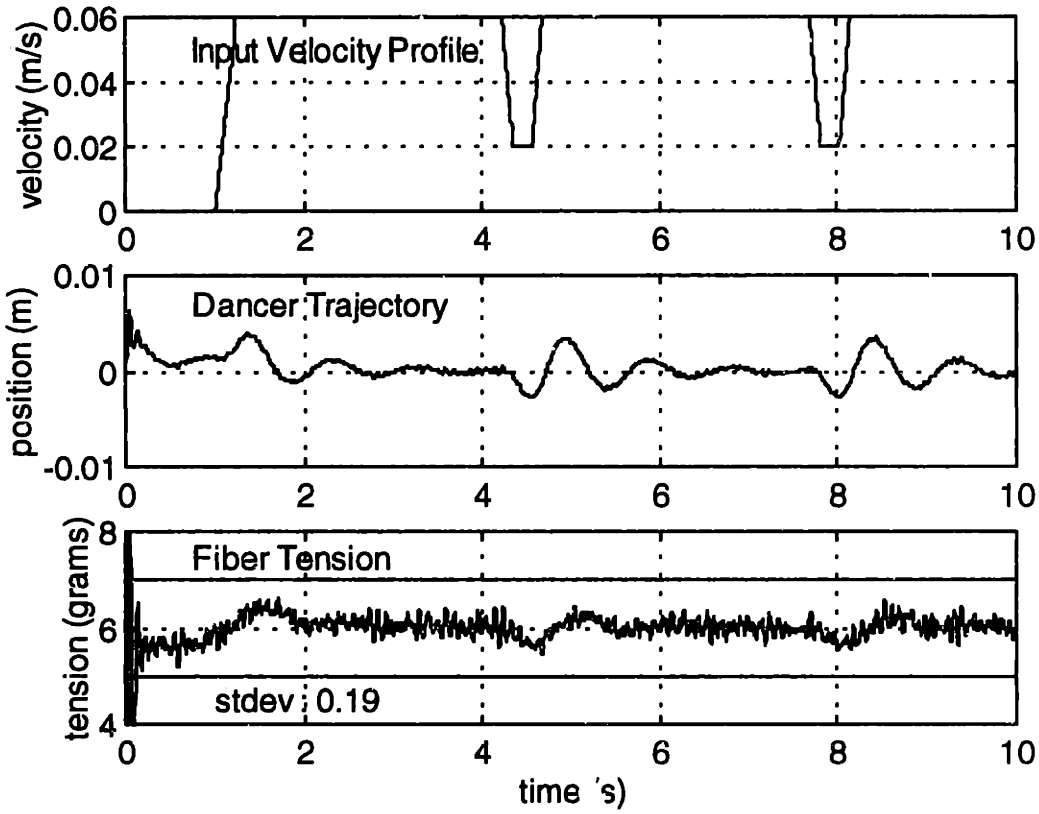

Figure 4.6 Winding Simulation with Feedback Noise.

The next simulation includes the coulomb friction of the dancer motor and also uses a slow zone winding profile. Coulomb friction tends to hold the dancer in place. Only when the applied force is larger than the frictional force will the dancer be able to move. As shown in Figure 4.7, coulomb friction slows the system response time and results in tension data with an increased standard deviation of 0.46 gram.

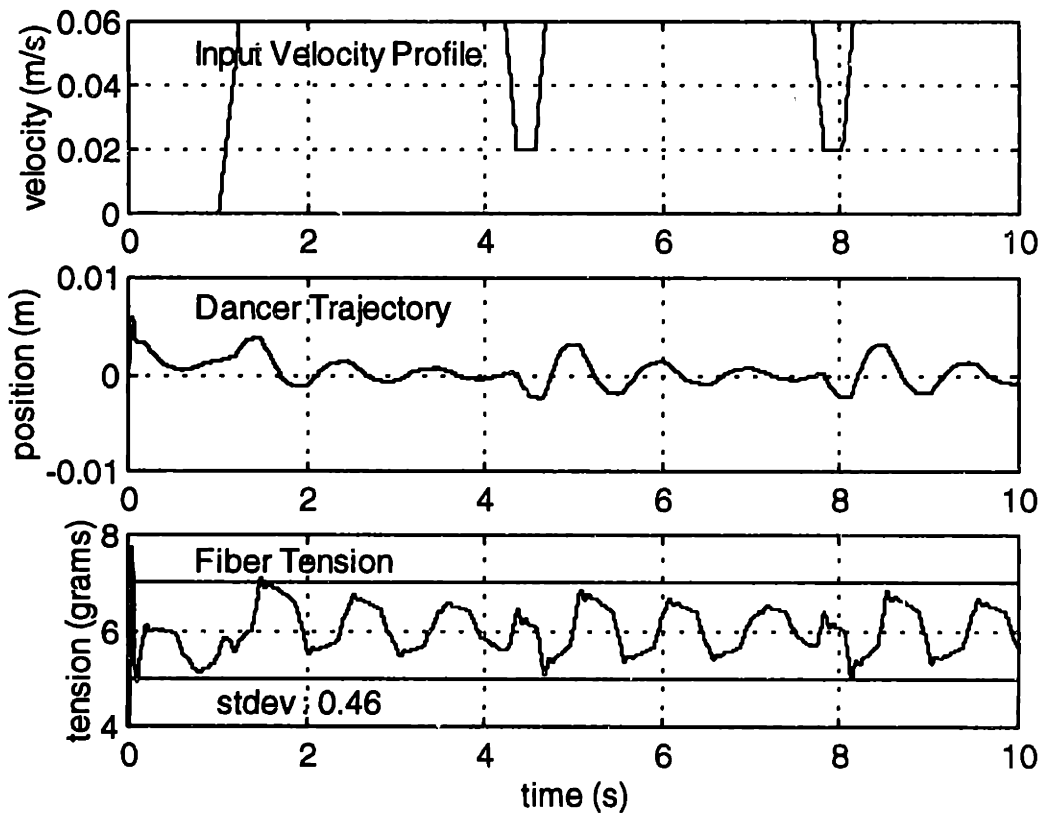

Figure 4.7 Winding Simulation with Coulomb Friction.

The result of adding noise into the system with coulomb friction is shown in Figure 4.8. The tension response actually improved over the simulation with just coulomb friction alone. The standard deviation decreases from 0.46 gram for the simulation without noise to 0.32 gram for the simulation with noise.

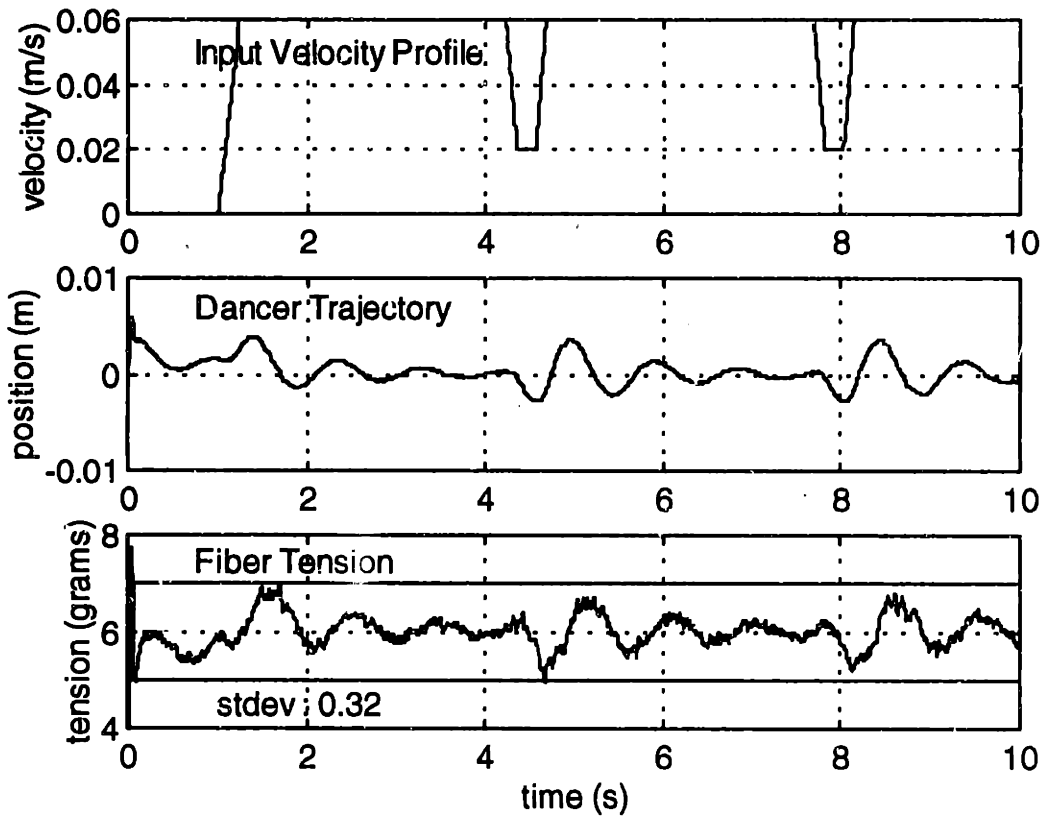

Figure 4.8 Winding Simulation with Noise and Coulomb Friction.

Observing the coulomb friction force and dancer command signal helps to explain this phenomena. Figure 4.9 shows the friction and dancer command signals for the simulation without noise. The effect of coulomb friction is most pronounced when the dancer is moving up or down. This is shown as square waves in the coulomb friction graph, which becomes a component of the dancer motor's command signal. These square waves cause the dancer arm to overshoot by applying force in addition to the PID control signal. When the dancer comes close to rest the coulomb friction fluctuates back and forth at high frequencies. The high frequency fluctuation essentially resembles noise and but is too fast for the dancer to respond to.

Once noise is injected into the feedback signal, the dancer vibrates up and down rapidly. Noise injection also causes the coulomb frictional forces to behave in a similar manner. From Figure 4.10, the load cell noise causes of square wave signals to fluctuate at higher frequencies in contrast to the case without noise (figure 4.9). It is this reduction in the number of low frequency square waves which improves the fidelity in tension control. Figure 4.10 also shows the addition of noise results in a dancer command signal that is smoother than the one without noise shown in Figure 4.9. So the addition of noise can act to suppress the transient error caused by the coulomb friction.

In the control of machine with nontrivial amounts of friction, a method called dithering is often used. This methods apply mechanical vibration to the mechanism that is plagued with friction. Through experimentation, dithering has demonstrated roughly a factor of three improvement in force control accuracy [Armstrong-Hélouvry]. The previous simulations have shown that noise in the feedback signal has similar effect on control of machines as applied dithering. In both cases, the impact of friction is reduced.

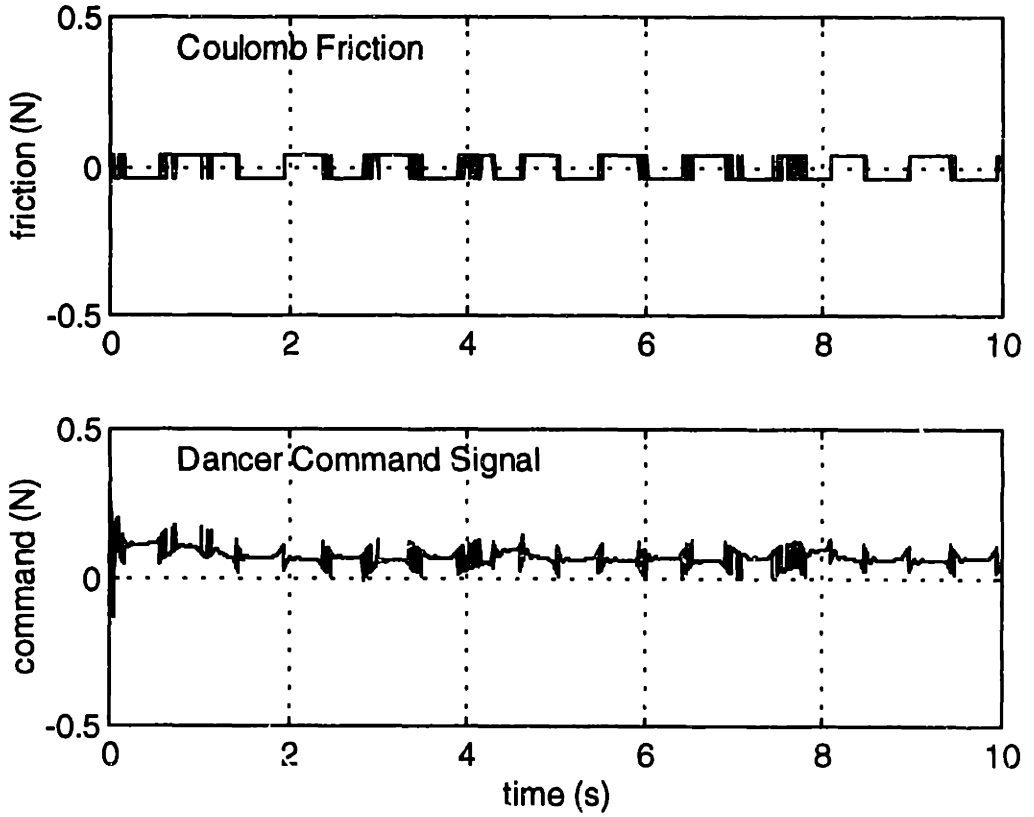

Figure 4.9 Effects of Coulomb Friction on Dancer Motor's Command Signal without Noise.

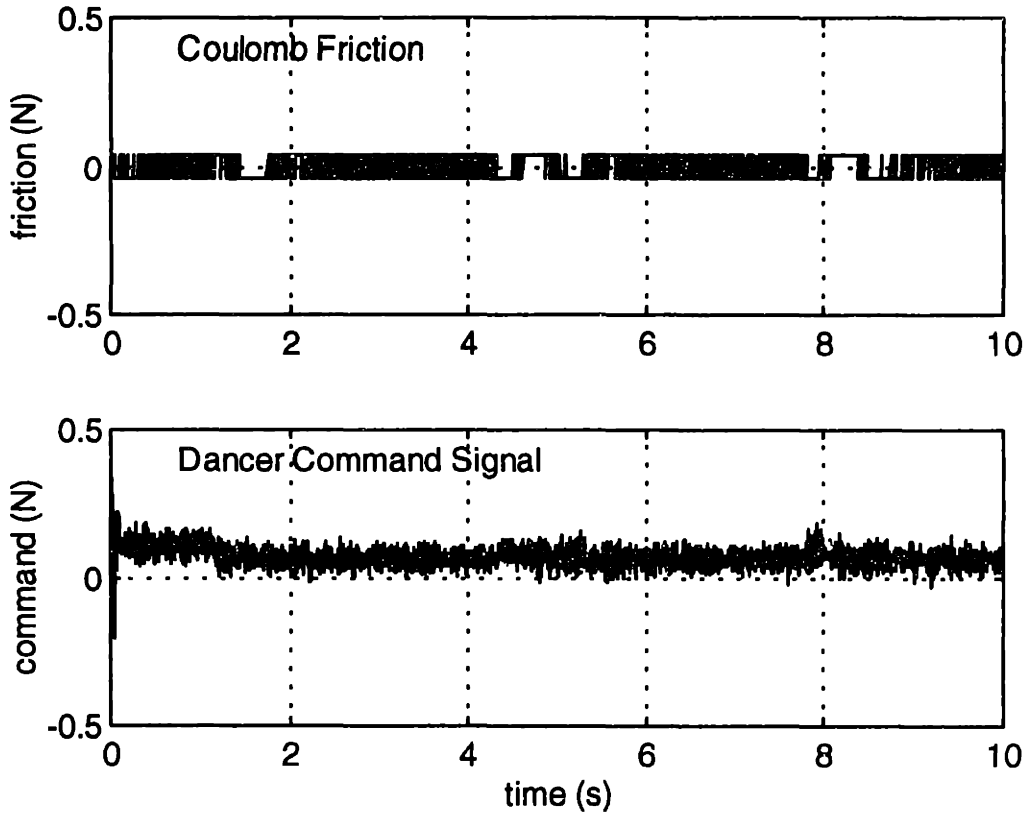

Figure 4.10 Effects of Coulomb Friction on Dancer Motor's Command Signal with Noise.

4.2 Feedforward Control alternative

4.2.1 Theory

From the results of the PID tension control simulations, it is evident that the tension data is dependent on the dancer position response. By reducing the transients in the dancer response, the transient of the tension response should also decrease. A candidate control alternative to PID control of the dancer position is disturbance feed-forward control [Ogata]. A Block diagram of a typical feedforward control loop appears in Fig 4.11. In disturbance-feed forward control, disturbances are approximately compensated for before they cause an error. On the other hand, feed back systems can only compensate for the

disturbance once an error materializes. This may take some time depending on the time constant of the plant involved. To take advantage of feedforward control, the disturbance must be measurable. Compensation for the disturbance is represented by the block labeled $G_f(s)$. Feedforward compensation schemes depend heavily on the consistency of the system's parameters. Any drift from these parameters can result in error. Another source of error is from unmeasured disturbances, since feedforward does not account for these disturbances. In order to compensate for parameter drift and unmeasureable disturbances, a PID feedback loop is still essential for accurate control.

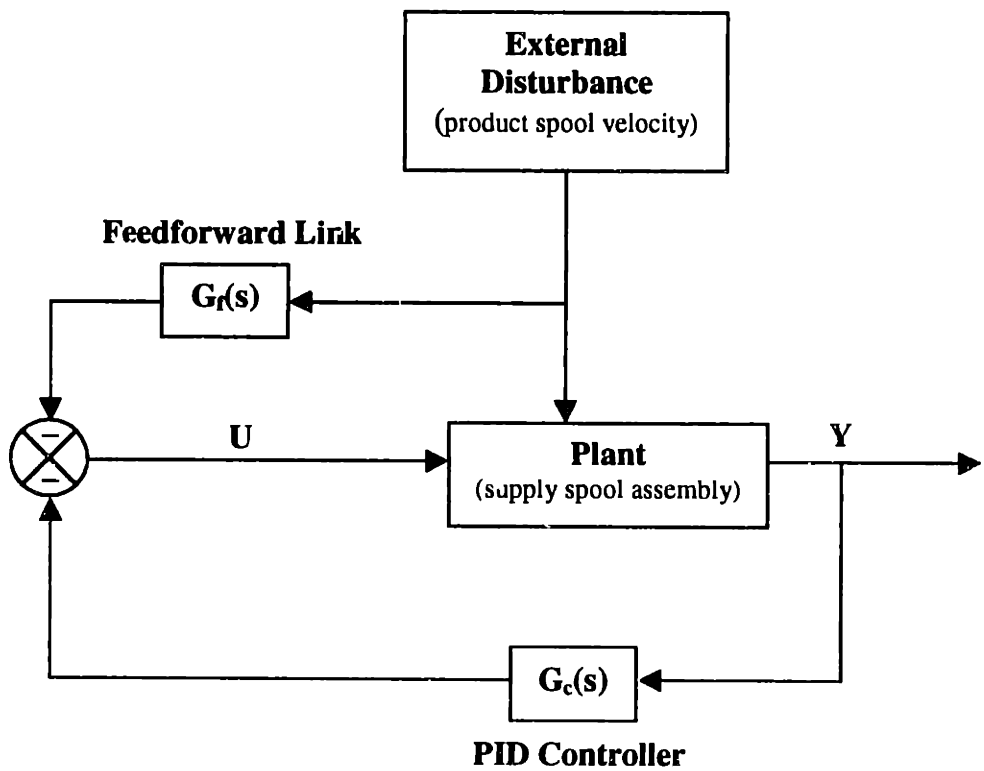

Figure 4.11 Typical Feedforward Control Loop.

4.2.2 Feed forward Simulink Model

Modifications were made on the Simulink model to implement feed forward controls. The feedforward control model is shown in Figure 4.12. Notice that the feedforward loop consists of a series of gains and derivative blocks to obtain a force that can ideally accelerate the supply spool as fast as the product spool. The feed forward input is then added to the PID control input to control the supply spool.

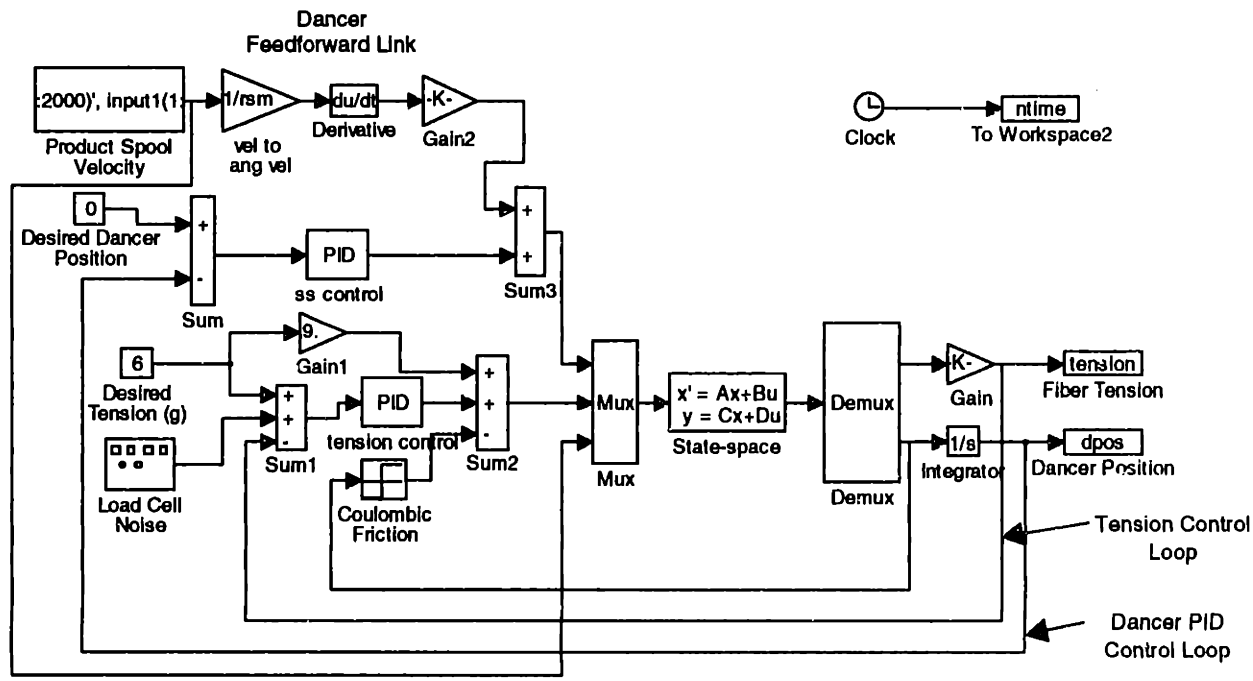

Figure 4.12 Feedforward Simulink Diagram.

4.2.3 Simulink results

The simulations applying feed forward to the tension control system are performed using system parameters as the PID control system. The first simulation represents winding at a constant speed. The results shown in Figure 4.13 indicate a slight improvement over the PID control shown in Figure 4.14. For a constant winding situation, disturbance

feedforward provides limited benefits since the disturbances from rapid acceleration and deceleration of the product spool are infrequent.

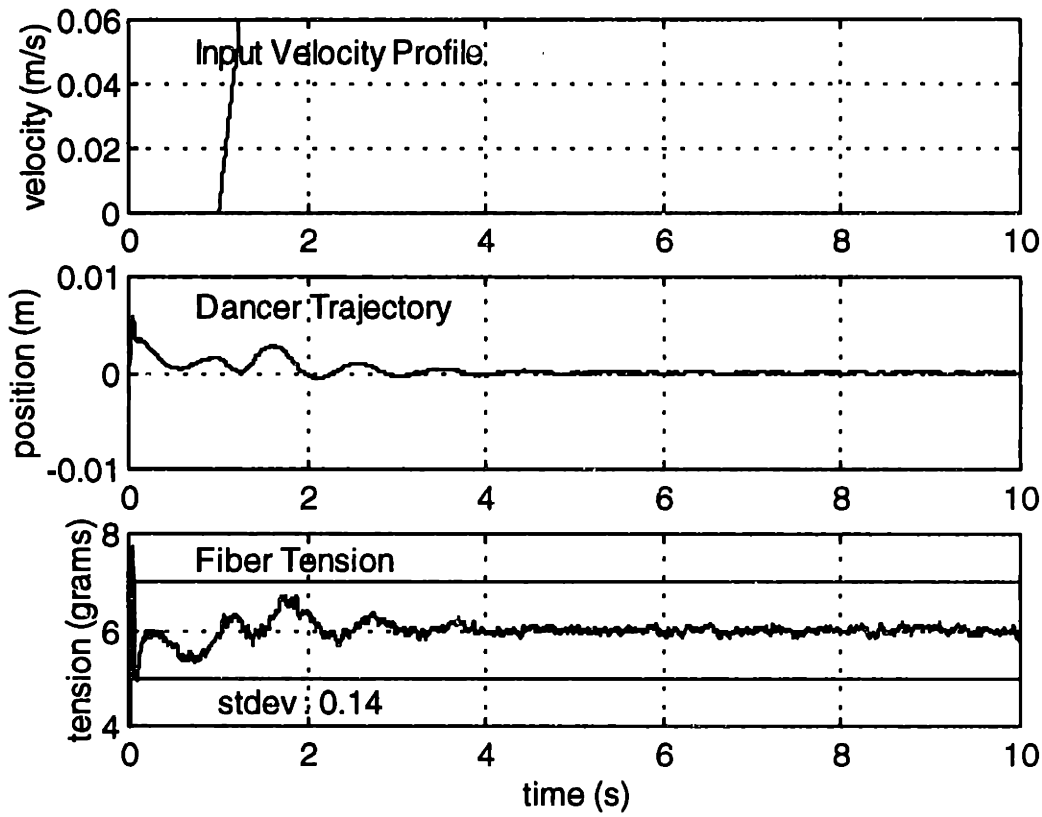

Figure 4.13 Winding Simulation at Constant Wind Speed Using Feedforward Control.

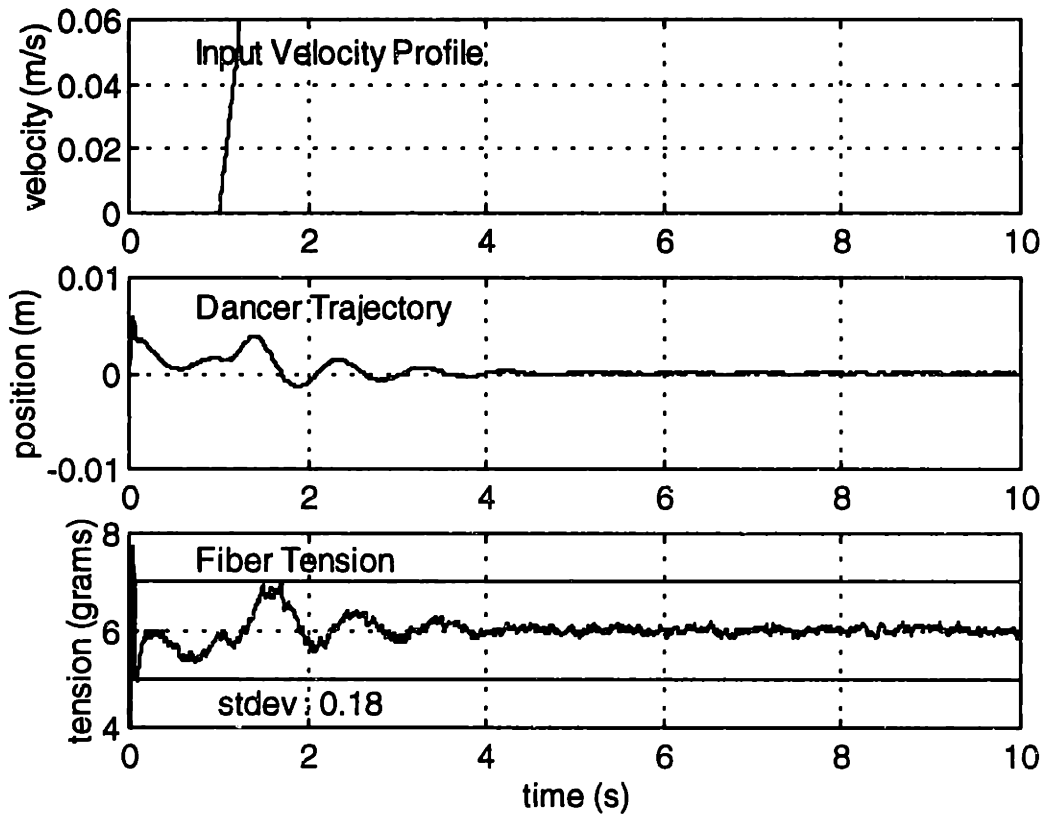

Figure 4.14 Wind Simulation at Constant Speed using PID Control.

The advantages of feedforward are more pronounced in the second simulation where slow zone winding is simulated. Results for this simulation are shown in Figure 4.15. The standard deviation of the tension transients due to acceleration is reduced from 0.32 gram for PID control to 0.24 gram for feedforward control. Although improvements to the system response exist, the improvements are not very dramatic. Feedforward does not compensate for the viscous friction modeled in the supply spool and dancer friction. For a system with no friction, feedforward can easily compensate for the disturbance, but for a system with friction, a time lag and transient error will still exist. Furthermore, unmeasured disturbances such as noise and coulomb friction, which both contribute to transient error, are still compensated for only by the PID feedback loop.

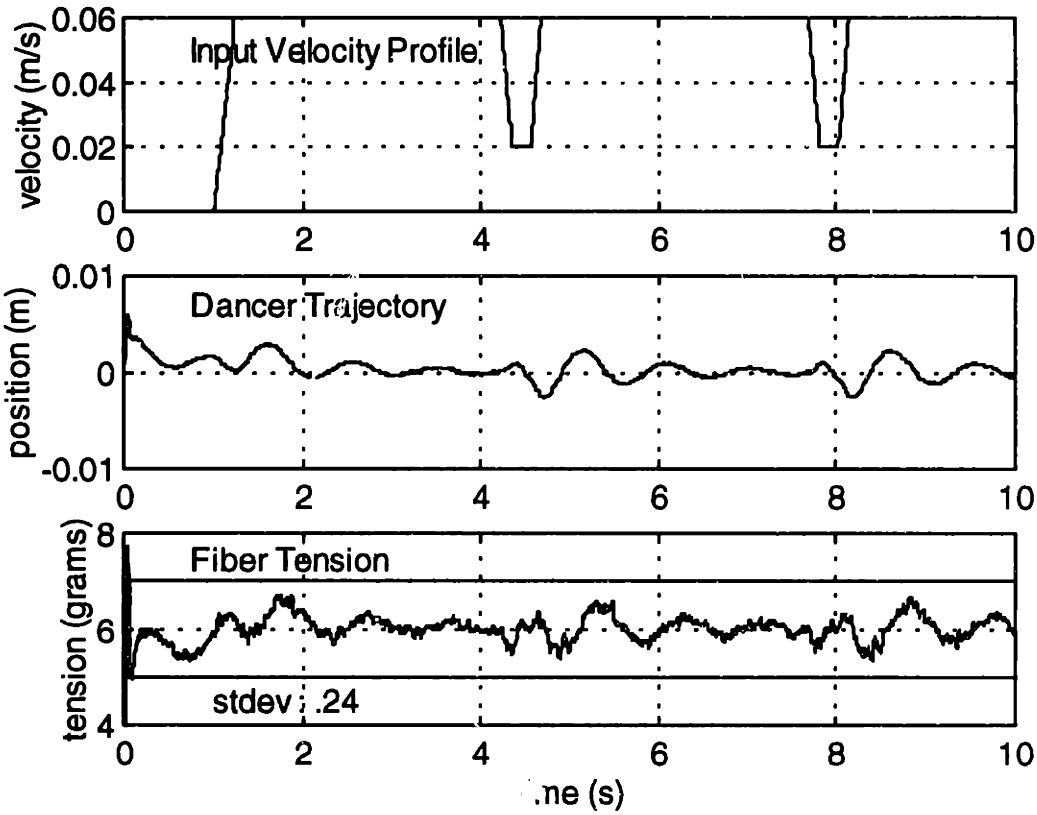

Figure 4.15 FeedForward Simulation with Slow Zone.

4.3 Experimental Results

The simulations provided conceptual information on the dynamics and performance of the tension control system. Experiments were performed on the final machine to verify and characterize the performance of the actual physical system. The data was collected by a Keithley Metrabyte™ 16-bit data acquisition board. The raw data was sampled at 500 Hz for a period of 10 seconds for each experiment. Since much of the high frequency tension transients are averaged out after the fiber is wound onto the coil, the data is averaged over 50 millisecond periods. The average data represent a more accurate representation of the fiber tension profile of the coil. Unless otherwise stated, all winding

experiments use a nominal wind speed of 90dps, a slow zone speed of 60dps and a target tension of 6grams.

4.3.1 Sensor Noise

The load cell signal is subject to both electrical and mechanical noise sources. Efforts were made to minimize load cell noise. First the signal amplifiers with 3kHz low-pass filters are placed as close as possible to the load cells. Secondly, the signal is read in using differential sampling methods to reject common mode noise. An example of load cell noise is shown in Figure 4.16. The raw data shown resulted in a standard deviation of 0.07 gram. Looking at the bottom graph, the major frequency components of the noise occurs at 17.03Hz and 59.62 Hz. The 17.03 Hz signal is due to the vibration that is transmitted to the supply units and load cells through the positioning system. The 59.62 Hz component resembles interference from AC power lines. However, through experimentation it was shown that the 59.62 Hz component is actually a result of the resonance of the main shaft. Vibration from the main shaft is transmitted to the load cell via the fiber connecting the product spool to the guide wheel.

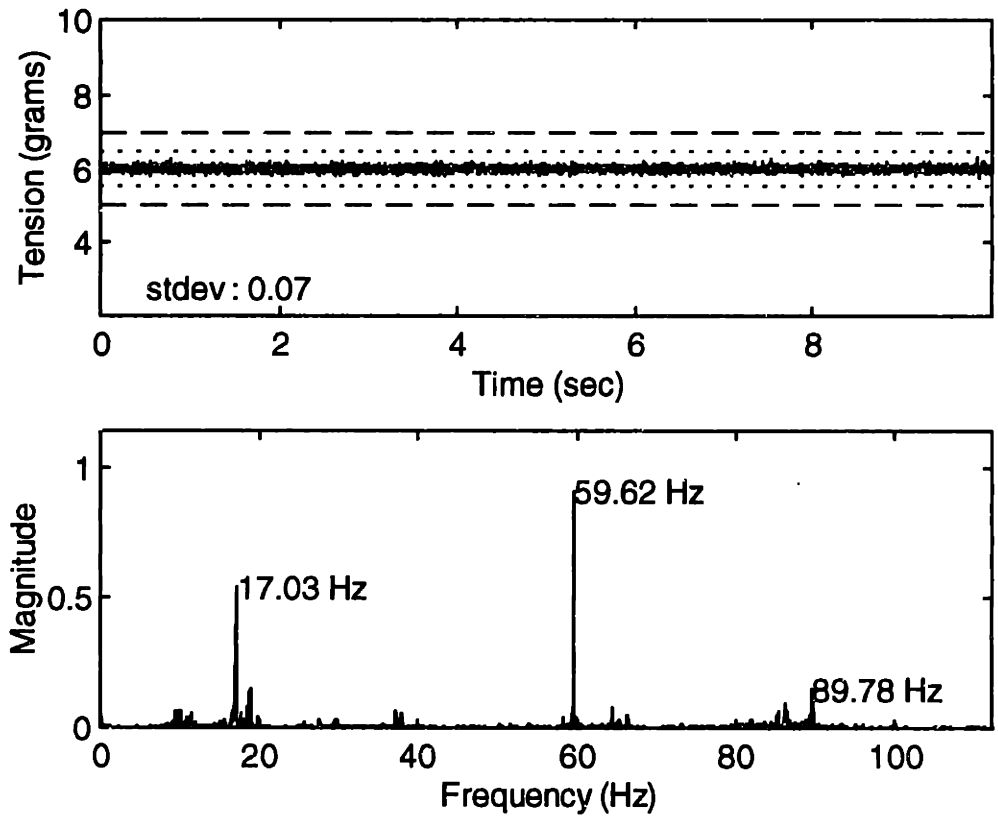

Figure 4.16 Load Cell Noise. Top: Noise sampled at 500 Hz. Bottom: Frequency Spectra of Noise Sampled.

The next two experiments show the effects of machine vibration on load cell noise. The top graph of Figure 4.17 represents load cell noise when the main shaft is spinning at 90 dps. In the experiment, the fiber is not attached to the spinning product spool so no winding occurs. The noise increases dramatically in this experiment. The standard deviation increases to 0.1544 gram.

Figure 4.18 represents noise in a typical winding experiment, except that no fiber is attached to the product spool for winding. This experiment adds an additional jog movement to the previous experiment described. The jog involves a coordinated move of the axis for every revolution of the product spool. The noise fluctuations at 2.2 and 6.6 sec correspond to the jogging of the supply unit. The noise at these points both break the ±1 gram lines shown. The experiments above show that load cell noise makes up a significant portion of the tension data collected.

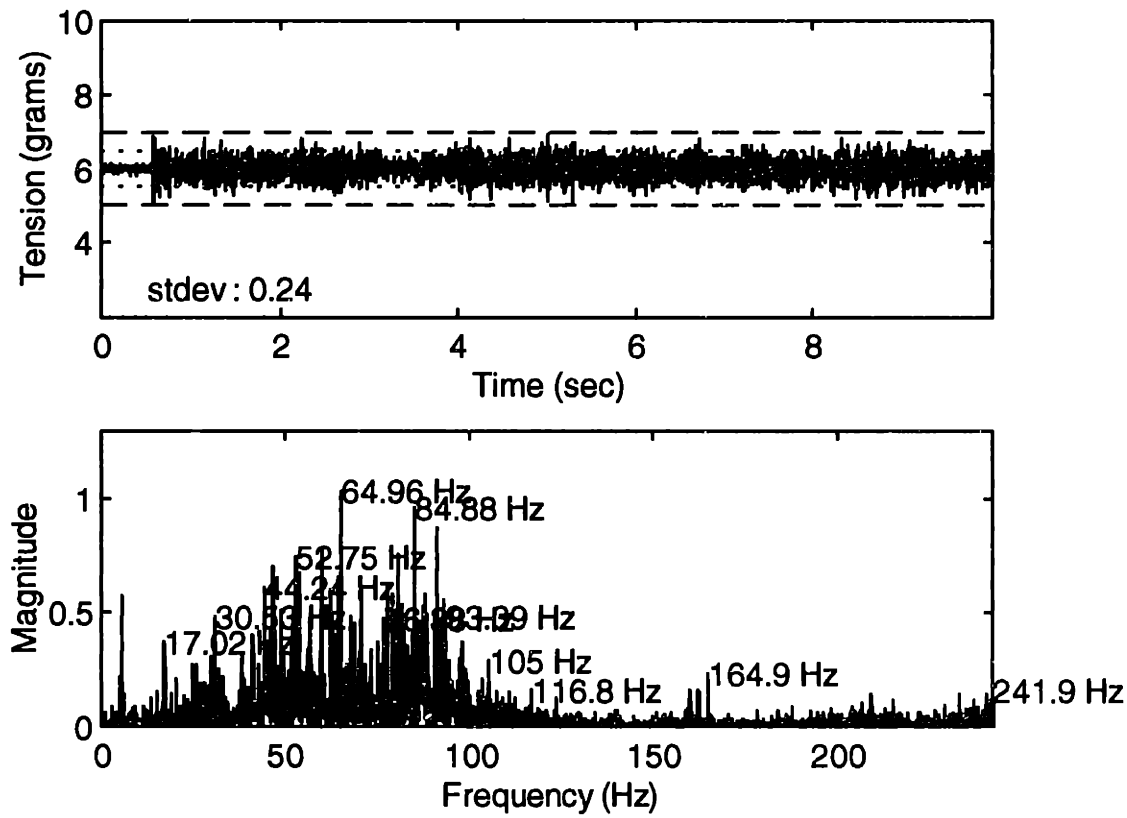

Figure 4.17 Load Cell Noise with Spinning Product Spool. Top: Noise sampled at 500 Hz. Bottom: Frequency Spectra of Noise Sampled.

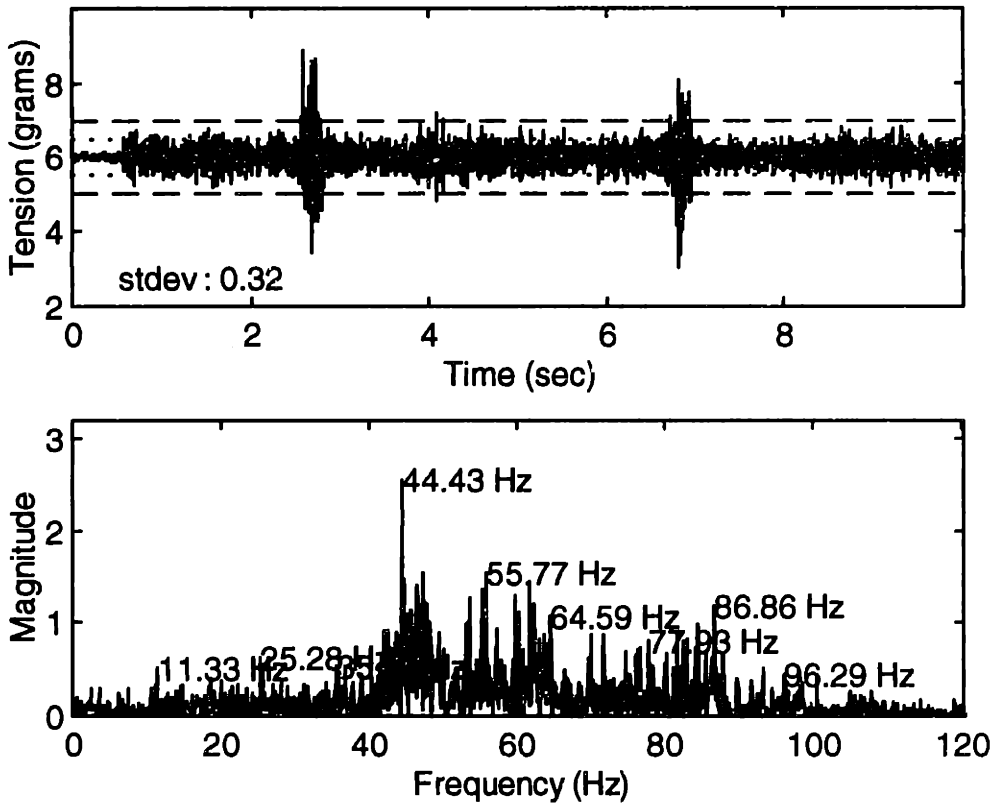

Figure 4.18 Load Cell Noise with Spinning Product Spool and Jog. Top: Noise sampled at 500 Hz. Bottom: Frequency Spectra of Noise Sampled.

4.3.2 PID Results

The first set of winding experiments control tension through PID control loops. Figure 4.19 shows tension data collected for a constant velocity wind. When the product spool initially accelerates at 0.6 sec, the tension increases, oscillates and settles down to the target tension. This behavior is also seen in the simulink simulation performed in section 4.2. For the most part the tension levels remain within ± 1 gram but occasionally escape these limits. The standard deviation of this experiment is 0.37gram.

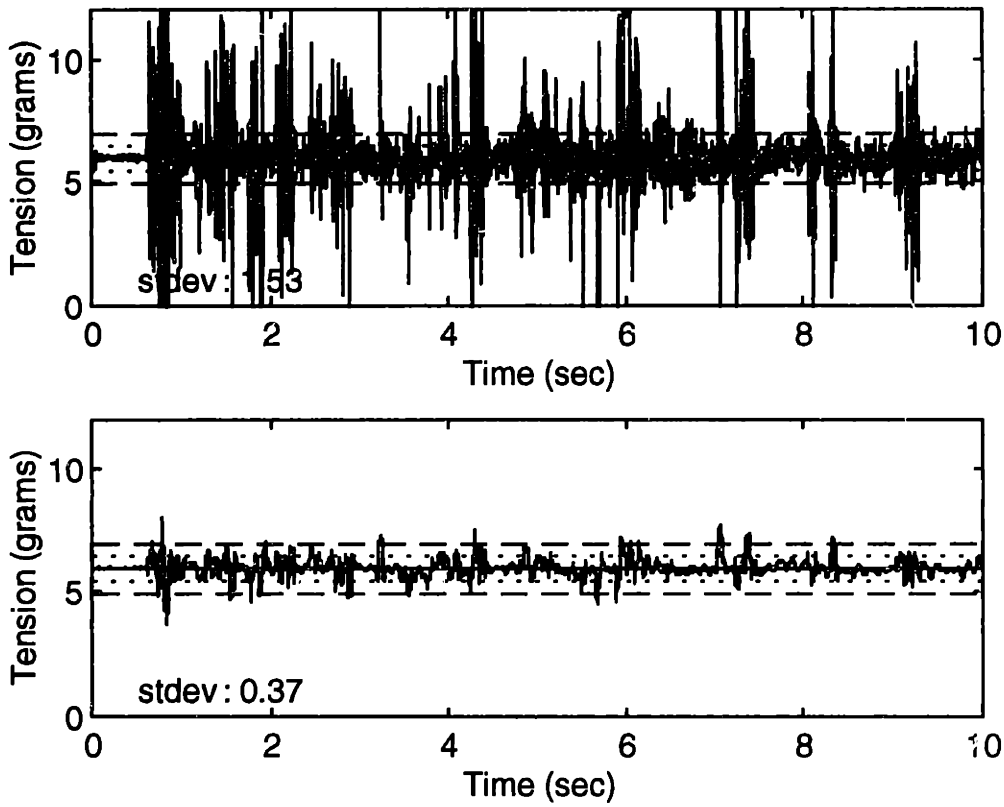

Figure 4.19 Winding at Constant Speed. Top: Raw Data Sampled at 500 Hz. Bottom: Data Averaged of 50 ms.

The Second experiment involves winding with a slow zone. The results are shown in Figure 4.20. Similar to the simulink results, the accelerations of the slow zone cause more transient errors in tension. The standard deviation increases to 0.49 gram. The large tension fluctuations at 3 and 7 seconds occur during the entering and exiting of the slow zone. Other than these large deviations, the tension control performs just as well as that of the previous experiment.

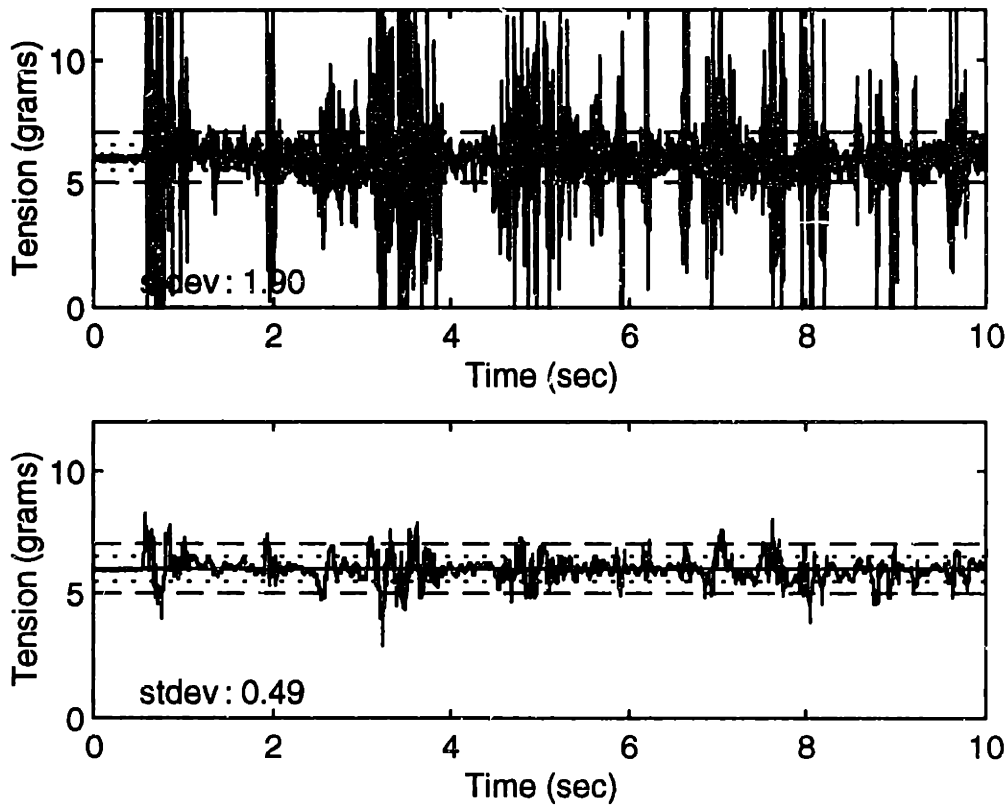

Figure 4.20 Winding with Slow Zone. Top: Raw Data Sampled at 500 Hz. Bottom: Data Averaged of 50 ms.

4.3.3 Feedforward results

The next set of winding experiments involve feedforward tension control. To implement feedforward control the acceleration of the product spool must be obtained. This is then used to calculate the supply spool motor's command signal. One approach is through software modification. However, the current motion controller does not have the flexibility to implement feedforward control. A second approach is used. Instead of software manipulation, modification of the electronics provides a way to implement feedforward control. The electrical circuit shown in Figure 4.21 is used in feedforward tension controls.

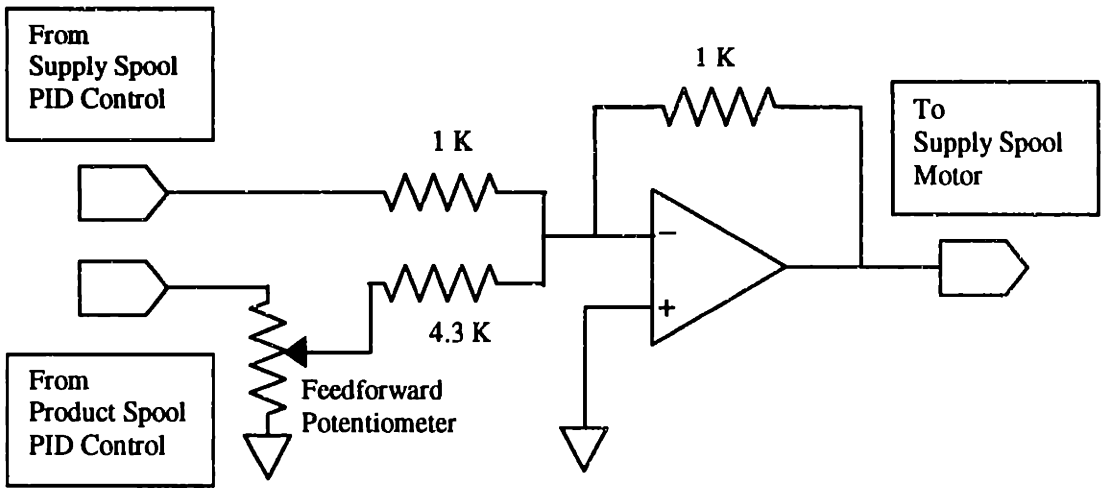

Figure 4.21 Feedforward Electrical Circuit.

This feedforward implementation assumes that the theta motor command signal is proportional to the acceleration of the product spool. In an ideal situation, the motor command signal is used as a reference that controls the motor current supplied by the amplifier. The motor current should be approximately proportional to the applied torque and thus the acceleration.

The potentiometer is tuned so that the tension transients are at a minimum and the PID loop gains are left unchanged. Ideally the feed forward link should compensate for the product spool disturbances and the supply spool PID loop should correct for the remaining uncertainties.

Again, two experiments using winding parameters similar to the PID experiments were performed in order to compare the results. Constant winding speed results are shown in Figure 4.22. The standard deviation of the raw data for feedforward is 1.24 grams compared to 1.53 grams for PID control. However, for the averaged data, the standard deviation for feedforward is 0.45 gram compared to 0.37 gram for PID. Overall,

feedforward control decreases noise and high frequency fluctuations, but increases low frequency fluctuations for the experiment with constant winding speed. The low frequency error is caused by deviation from implementation of ideal feedforward control. The theta PID loop not only provides the torque to accelerate the product spool, but also the torque needed to compensate for external disturbances inherent to the theta axis. One such disturbance is the unbalanced weight of the ride clamps that applies a torque on the theta axis. The ride clamps apply a torque that varies sinusoidally as the theta axis or main shaft spins. The sinusoidal response seen in the feedforward data could be the result of an attempt by the theta PID loop to compensate for the ride clamps' weight.

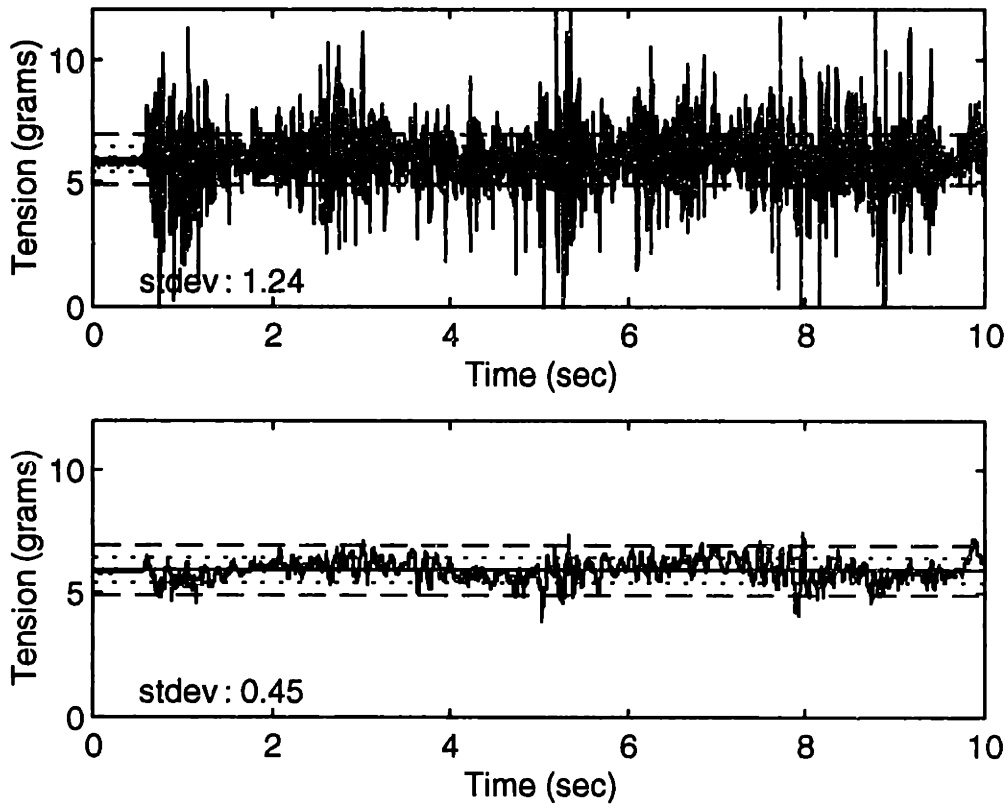

Figure 4.22 Feedforward Results with Constant Winding Speed. Top: Raw Data Sampled at 500 Hz. Bottom: Data Averaged of 50 ms.

The second feedforward experiment used a winding profile with slow zones. The standard deviation of both raw data and averaged data is reduced compared to PID control. The tension collected is shown in Figure 4.23. At approximately 3 and 7 seconds, the tension fluctuation did not increase significantly during the slow zone. This contrast with the results generated by the PID controller. Feedforward control is able to compensate for the disturbance of product spool before large transient errors materialize.

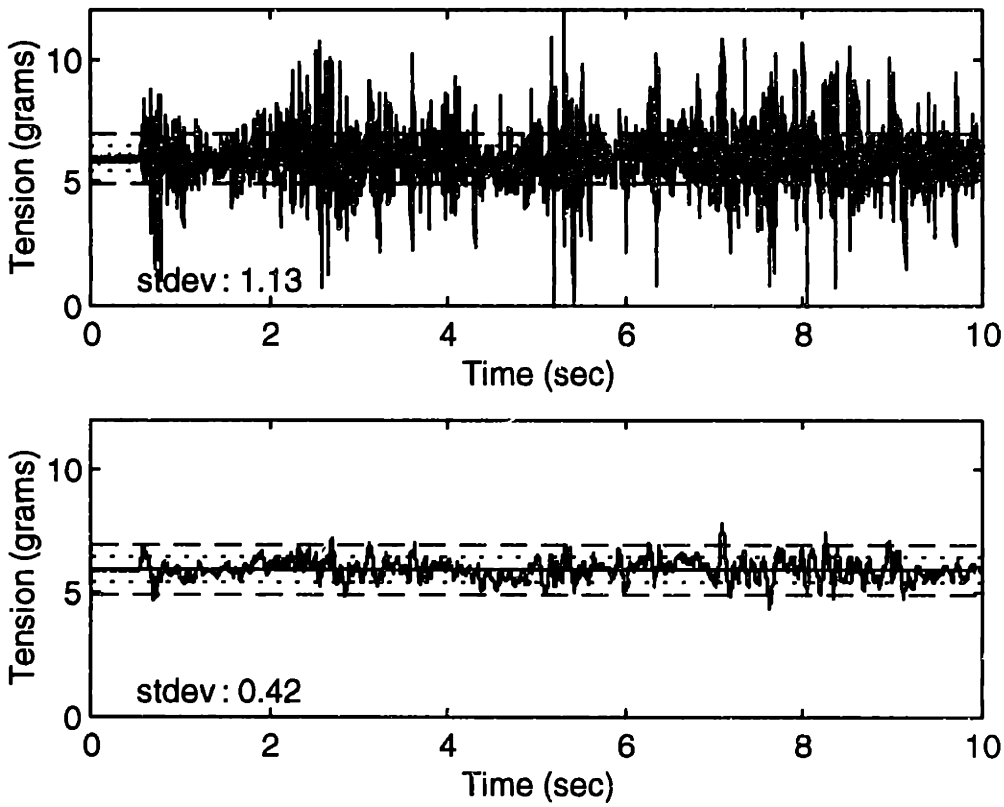

Figure 4.23 Feedforward Results with Slow Zone. Top: Raw Data Sampled at 500 Hz. Bottom: Data Averaged of 50 ms.

In feedforward control, use of the theta PID command signal is advantageous to using the actual product spool acceleration values. The simulated feedforward loops do not compensate for the viscous friction of the supply motors. Compensation for viscous friction is provided by the supply spool PID controller. Since the theta PID loop also compensates for viscous friction of the theta axis, using the theta PID command for feedforward may also help compensate for the supply spool friction. This may be the reason for the reduction of transient errors during constant winding speeds.

The experimental results above demostrates the distinct advantage of feedforward over PID control in distrubance rejection. However, efforts must be taken to measure the

disturbance accurately and to exclude measurement of other external factors. Measurement errors can lead to degradation of system performance as seen in the constant speed winding experiments. Software instead of electrical implementation should be used to obtain a more accurate representation of the product spool disturbance. However, the winder's equipment makes feedforward software implementation prohibitive. With this information, it was decided that PID would provide better tension control for winding experimental coils. Since throughput is not as important as minimizing tension transients, winding at a constant speed is acceptable. Using PID control in conjunction with a constant winding speed provides the best tension control performance.

5 Conclusion

A photograph of the automated FOG coil winder is shown in Figure 5.1. The machine was operational by the end of 1997. In March of the following year, the winder was delivered to the customer's facilities. Currently, the machine is being utilized to test the effects of varying mandrel designs and properties. Testing in the future will take advantage of the flexibility of the coil winder by varying the winding parameters and patterns used.

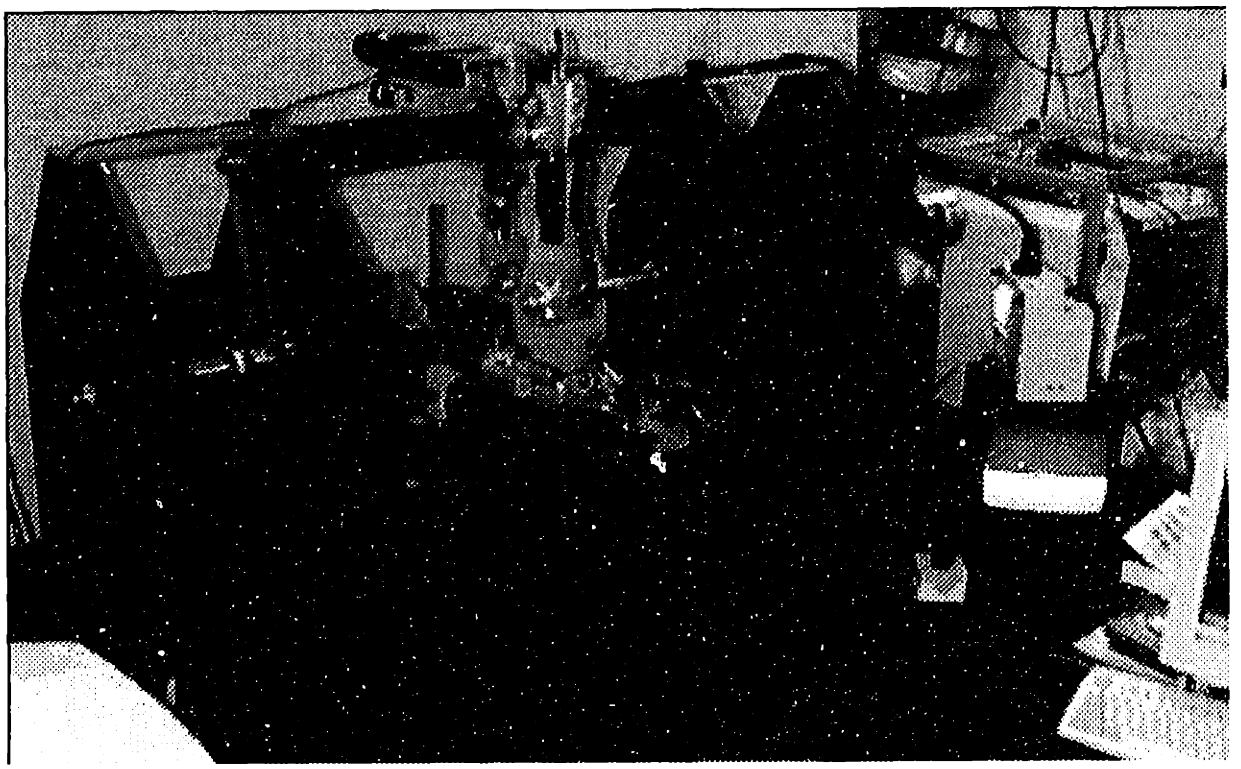

Figure 5.1 Final Delivered Machine.

The successful and timely completion of the winder was due to several factors. The original design gave the development team a solid foundation, on which to base the current design of the winder. Several subsystems such as the supply unit and ride clamp

were enhanced to improve the performance of the winder. An additional subsystem, the active ride system, has also been incorporated. With the software and electrical modifications, the active ride system is able to consistently and accurately control the tension during any winding situation. The above mentioned factors allow the winder to produce strategic grade FOG coils in an automated fashion.

The winder has proved to be successful in meeting product requirements. However, there is still room for improvement. More successful feedforward control results can be obtained if the errors originating from the ride clamp mass can be eliminated. This can be accomplished by balancing the ride clamps through the attachment of a counterbalance weight.

Tension control may also be improved through learning control. This method would make use of the data collected in previous operations to adapt and update the control gains. This ability to adapt would enable the winder to improve tension control performance. This type of control would be most effective in controlling tasks that are highly repetitive such as winding several turns of a FOG coil.

Both suggestions can be incorporated into future winders to help improve the quality and accuracy of the FOG coils produced.

6 References

1. Karnopp, Margolis and Rosenberg, *System Dynamics: A Unified Approach*, Second Edition, Jogn Wiley & Son, Inc., New York, New York, 1990.

2. Dakin and Culshaw, *Optical Fiber Sensors Applications, Analysis, and Future Trends*, Volume Four, Artech House, Norwood, Massachusetts, 1997 (p. 197).

3. Wrigley, Hollister and Denhard, *Gyroscopic Theory, Design, and Instrumentation*, The M.I.T Press, Cambridge, Massachusetts, 1969 (pp. 4-5).

4. Ogata, *Modern Control Engineering*, Third Edition, Prentice-Hall, Upper Saddle River, New Jersey, 1997 (pp.700-703).

5. "Design and Development of an Automated Fiber Optic Gyroscope Coil Winding Machine," Stephan M. Lin, Thesis (M.S.), MIT, Department of Mechanical Engineering, 1997.

6. "Enhancement and Development of an Automated Fiber Optic Gyroscope Coil Winding Machine," Jesse C. Darley, Thesis (M.S.), MIT, Department of Mechanical Engineering, 1998.

7. Krohn, *Fiber Optic Sensors Fundamentals and Applications*, Second Edition, Instrument Society of America, Research Triangle Park, North Carolina, 1992 (pp. 223-236).

8. Burns, *Optic Fiber Rotation Sensing*, Academic Press, Inc., San Diego, California, 1994 (pp.7-8).

9. Horowitz and Hill, *The Art of Electronics*, Second Edition, Cambridge University Press, New York, New York, 1989 (pp. 1-200).

10. Armstrong-Hélouvry, *Control of Machines with Friction*, Kluwer Academic Publishers, Boston, Massachusetts, 1991 (p.162).